Multipoint observations of ionic structures in the Plasmasphere by CLUSTER - CIS and comparisons with IMAGE-EUV observations and with Model Simulations

Iannis Dandouras (1), Viviane Pierrard (2), Jerry Goldstein (3), Claire Vallat (1), George K. Parks (4), Henri Rème (1), Cécile Gouillart (1), Fréderic Sevestre (1), Michael McCarthy (5), Lynn M. Kistler (6), Berndt Klecker (7), A. Korth (8), M. B. Bavassano-Cattaneo (9), Philippe Escoubet (10), Arnaud Masson (10)

(1) Centre d'Etude Spatiale des Rayonnements, Toulouse, France

(2) Belgian Institute for Space Aeronomy, Brussels, Belgium

(3) SWRI, San Antonio, TX, USA

(4) Space Science Laboratory, UC Berkeley, CA, USA

(5) Geophysics, University of Washington, Seattle, WA, USA

(6) University of New Hampshire, Durham, NH, USA

(7) Max-Planck-Institut für Extraterrestrische Physik, Garching, Germany

(8) Max-Planck-Institut für Aeronomie, Katlenburg-Lindau, Germany

(9) IFSI, Rome, Italy

(10) ESA/ESTEC RSSD, Noordwijk, The Netherlands

Submitted to: Yosemite 2004 AGU Monograph

May 2004

ABSTRACT

The 4 Cluster spacecraft orbit the Earth in a highly eccentric polar orbit at 4 R_E perigee, and this permits them to sample the ring current, the radiation belts and the outer plasmasphere. Data provided by the Cluster Ion Spectrometry (CIS) instruments are used to analyze Cluster crossings of the plasmasphere. CIS is capable of obtaining full three-dimensional ion distributions (about 0 to 40 keV/q) with a time resolution of one spacecraft spin (4 sec) and with mass-per-charge composition determination. In addition the CIS Retarding Potential Analyser (RPA) allows more accurate measurements in the about 0 - 25 eV/q energy range, covering the plasmasphere energy domain. The low-energy ion distribution functions, obtained by CIS-RPA during the perigee passes, allow to reconstruct statistically the plasmapause morphology and dynamics, but they also reveal new and interesting features. The ion discrimination capability of CIS reveals how the density profile is different for each of the main ion species (H^+, He^+, O^+): H^+ and He^+ present mostly similar profiles; O^+, however, is not observed as trapped plasmaspheric population at the Cluster orbit altitudes ($R \geq 4\ R_E$). Low-energy O^+ is observed mainly as upwelling ion, on auroral field lines. Detached plasmasphere events, that are observed by CIS during some of the passes at about 0.5 to 1 R_E outside the plasmapause, are also present. The bi-directional distribution functions of these detached plasmaspheric populations allow us to distinguish them from upwelling ion populations. The CIS-RPA observations of the plasmapause position have been simulated with an interchange instability numerical model for the plasmapause deformations, and the model reproduces in a very satisfactory way the CIS observations. The CIS local ion measurements have also been correlated with global images of the plasmasphere, obtained by the EUV instrument onboard Image, for an event where the Cluster spacecraft were within the field-of-view of EUV. The EUV images show, for this event, that the difference observed between two Cluster spacecraft was temporal (boundary motion): the radial density profile of

the plasmasphere varies with MLT, and a more extended radial profile "rotated" into between the two Cluster spacecraft perigee passes. They thus show the necessity for correlating local measurements with global images, and the complementarity of the two approaches; local measurements giving the "ground truth" (including plasma composition, distribution functions etc.) and global images allowing to put local measurements into a global context, and to deconvolve spatial from temporal effects.

1. INTRODUCTION

The plasmasphere is the torus of cold (~1 eV) dense plasma, that encircles the Earth occupying the inner magnetosphere out to a boundary known as the plasmapause, where the density can drop by 1 to 2 orders of magnitude. The configuration and dynamics of the plasmasphere are highly sensitive to geomagnetic disturbances. During extended periods of relatively quiet geomagnetic conditons the outer plasmasphere can become diffuse, with a gradual fall-off of plasma density. During increasing magnetospheric activity, however, the plasmasphere is eroded and plasmaspheric ions can be peeled off and escape toward the outer magnetosphere.

The outer plasmasphere region is located at the interface between the expanded ionosphere, corotating with the Earth, and the internal magnetosphere, dominated by sunward convection [e.g. *Lemaire and Gringauz,* 1998]. In contrast with the inner plasmasphere, where the density repartition is smooth, the outer plasmasphere is characterized by complex plasma structures, formed by fluctuations of the convective large-scale electric field governed by solar wind conditions. Observations and modelling efforts have demonstrated that, for instance, plasma tongues can be wrapped around the plasmasphere, shoulders can be formed, or that plasma irregularities can be detached from the main body of the plasmasphere [*Lemaire,* 2001; *Goldstein et al.,* 2003a; *Sandel et al.,* 2003]. The in situ observations of the outer plasmasphere obtained by the Cluster constellation provide some novel views of this region.

In this study we will use data provided by the Cluster Ion Spectrometry (CIS) experiment [*Rème et al.,* 2001] to analyze the ionic structures observed locally during the Cluster spacecraft crossings of the plasmasphere. The perigee of the four Cluster spacecraft, at ~4 R_E, allows cuts through the outer plasmasphere. The CIS observations of the plasmapause position are then compared to the simulation results using an interchange instability numerical

model for the plasmapause deformations [*Pierrard and Lemaire,* 2004]. The CIS local ion measurements have also been correlated with global images of the plasmasphere, obtained by the EUV instrument onboard Image [*Sandel et al.,* 2000], for an event where the Cluster spacecraft were within the field-of-view of EUV (Figure 1).

2. CLUSTER ORBIT AND INSTRUMENTATION

The Cluster mission is based on four identical spacecraft launched on similar elliptical polar orbits with a perigee at about 4 R_E and an apogee at 19.6 R_E [*Escoubet et al.*, 2001]. This allows Cluster to cross the ring current region, the radiation belts and the outer plasmasphere, from South to North, during every perigee pass. Orbital manoeuvres that change the inter-spacecraft separation take place once or twice per year, allowing the study of different characteristic scales in the various plasma regions in the magnetosphere and in the solar wind. The tetrahedron formed by the four spacecraft can thus have characteristic sizes ranging between 100 km and more than 10 000 km.

The Cluster Ion Spectrometry (CIS) experiment on board Cluster consists of the two complementary spectrometers CODIF (or CIS-1) and HIA (or CIS-2), and provides the three-dimensional ion distributions (from about 0 to 40 keV/q) with one spacecraft spin (4 seconds) time resolution [*Rème et al.,* 2001]. Furthermore, the mass-resolving spectrometer CODIF provides the ionic composition of the plasma for the major magnetospheric species (H^+, He^+, He^{++} and O^+), from the thermal energy to about 40 keV/q. In addition CODIF is equipped with a Retarding Potential Analyser (RPA), which allows more accurate measurements in the about 0.7 - 25 eV/q energy range, covering the plasmasphere energy domain. The operation on CODIF of the RPA mode and of the normal magnetospheric modes (which provide a 25 eV/q to 40 keV/q energy range) is mutually exclusive. The RPA mode is thus operated on one out of 10 orbits, on the average, and not always on all of the spacecraft.

The magnetic field data, used here to calculate ion pitch angle distributions, come from the FGM (Fluxgate Magnetometer) experiment on board Cluster [*Balogh et al*., 2001].

The Image spacecraft was launched in March 2000 into an elliptical highly inclined orbit with an apogee altitude of 7.2 R_E and a perigee altitude of 1000 km [*Burch,* 2000]. On board Image, the Extreme Ultraviolet Imager (EUV) provides global images of the plasmasphere, by imaging the distribution of He^+ in its 30.4 nm resonance line [*Sandel et al.,* 2000].

3. OBSERVATIONS AND ANALYSIS

3.1 Plasmasphere Cut: 4 July 2001 Example

Figure 2 shows an example of a Cluster crossing of the plasmasphere, in the post-noon sector (15:30 MLT), during quiet magnetospheric conditions (4 July 2001 event: Kp = 1+). Figure 3 shows the corresponding orbit plot. During this event CODIF (bottom 3 spectrograms in Figure 2) was in the RPA mode (~0.7 - 25 eV/q) until 16:00 UT, when it switched back to a normal magnetospheric mode (full energy coverage). HIA (top spectrogram in Figure 2) was continuously in a normal magnetospheric mode. Cluster was in the southern lobe until ~10:20 UT, when it crossed a first boundary, entering into the southern plasma sheet (cf. HIA data). At ~10:45 UT the spacecraft entered into the ring current, where it remained until ~13:40 UT, characterized in these data by intense particle fluxes at energies above 7 keV, showing the presence of high-energy ions subject to gradient and curvature drift [*Vallat et al.*, 2004]. The spacecraft then through the northern plasma sheet, entered into the northern lobe, at the outbound leg of its trajectory, at ~14:38 UT.

Between 11:30 and 12:55 UT HIA suffered from a strong background from the radiation belts, due to penetrating particles, appearing as a high counting rate for all energies.

This background presents two maxima centered on L-shell values around 4.5, one at the inbound leg and the other at the outbound leg of the orbit.

CODIF, which during this event was in the RPA mode, first detected the presence of a diffuse low-energy ion population at 11:00 UT, and then entered into the main plasmasphere at 11:30 UT. This is characterized by high ion fluxes at energies below 7.7 eV/q, with respect to the spacecraft potential. As will be shown later, the Cluster spacecraft potential in the plasmasphere is of the order of 1-2 V. The plasmaspheric ion data shown here cover thus an energy domain of ~2 to ~9 eV, and they correspond to the tail of the distribution function, which in the plasmasphere has typical temperatures of the order of 1 eV [*Comfort,* 1996; *Bezrukikh et al.,* 2001]. The plasmasphere is detected until about 13:00 UT, in the outbound leg, corresponding to geocentric distances below 4.6 R_E.

Ionic composition is provided by CODIF thanks to the time-of-flight technique, where ions, after being accelerated through a 15 kV potential, have their velocity measured by measuring the time-of-flight of each ion through a given length. The spectrograms plotted in Figure 2, for three main ion species, correspond each to the time-of-flight interval of the given species. In order to check the mass separation and the eventual contamination by background, we ploted, in Figure 4, a time-of-flight spectrum for the ions detected between 11:30 and 12:40 UT. The characteristic picks of H^+ and He^+ are clearly present. He^{++}, if present, would be almost "washed-out" by the tail of the H^+ distribution (spillover). Note that for H^+ the height of the pick is not proportional to the relative abundance, because a different sampling low was used, in the spectrum, for H^+ and for the other ion species. Figure 4, however, does not show the presence of O^+ ions (although it cannot be completely excluded). A persistent background is present over all energy channels, due to penetrating particles from the radiation belts, and it produces the two faint yellow strips shown in the O^+ spectrogram of Figure 2. O^+, if present, should have an extremely low signal-to-noise ratio. Note also that the radiation

belt background is relatively low, due to the time-of-flight technique that eliminates a large number of counts from penetrating particles, and it allows the clear identification, in this event, of dominant species such as H^+ and He^+. This is not the case with HIA, which does not use the time-of-flight technique, and where the radiation belt background can become overwhelming (cf. upper panel of Figure 2).

The moments of the ion distribution functions, calculated in the ~0.7 eV/q to 25 eV/q energy range (with respect to spacecraft potential), are shown in Figure 5a for H^+ and in Figure 5b for He^+. The densities present similar profiles for these two ion species, with the He^+ densities being lower by a factor of ~15, consistently with the measurements by DE 1 for the same geocentric distance [*Craven et al.,* 1997]. Note the characteristic density drop at the plasmapause, by about one to two orders of magnitude. The absolute values of the densities measured here are comparable, but slightly lower, to those usually measured onboard Cluster by the Whisper resonance sounder experiment [*Décréau et al.,* 2001; *Moullard et al.,* 2002; *Darouzet et al.,* 2003], because CODIF-RPA measures particles only in a finite energy range.

The H^+ and He^+ velocities measured here show a clear $Vx < 0$ and a $Vy > 0$ component, consistent with a corotating plasma, given the spacecraft position at 15:30 MLT (theoretical corotation velocity: 2.1 km s^{-1}). The systematic bias to negative values, shown by the Vz component, is the artefact of the instrument particle detection efficiency being inhomogeneous across the anodes looking on different elevations, and not completely compensated by the calibration values.

The H^+ and He^+ temperatures within the plasmasphere show typical values of 1 eV. Outside the plasmaspheric dense plasma the temperature and velocity calculations suffer from reduced counting statistics.

3.2 Detached Plasmasphere Observations: 31 October 2001 Event

Figure 6 shows a crossing of the plasmasphere by Cluster spacecraft (sc) 1, 3 and 4, in the morning sector (08:45 MLT), during initially quiet magnetospheric conditions (31 October 2001 event: Kp = 0+ during the 9-12 UT interval). The onset of a negative auroral bay is however observed in the AE index at ~12:30 UT, i.e. close to the outbound plasmapause crossing by the Cluster spacecraft, and the Kp index jumped from 0+ to 3 in the 12-15 UT interval.

All spacecraft were in the RPA mode. Cluster sc 3 was lagging on its orbit, with respect to the other spacecraft, which explains why it crossed the plasmasphere about 30 minutes later. Sc 1 and 4 crossed the plasmaspheric main ion population between ~10:47 UT ($L \approx 5.1$) and ~12:04 UT ($L \approx 5.8$). However, detached plasma of lower density was also observed before the entry into the main plasmasphere, at around 10:00 UT ($L \approx 11$), and after the exit from the plasmasphere, at around 12:25 UT ($L \approx 8$) and at around 13:30 UT ($L \approx 55$).

The bottom panel of Figure 6 shows the H^+ pitch-angle distributions (pad) for sc 4. The distributions in the main plasmasphere are relatively isotropic, while around the crossing of the equatorial plane the major part of the proton population is centred at 90° (pancake distributions). On the detached plasmasphere observations, however, the distributions are still trapped (distributions symmetric with respect to the magnetic field), but are of the butterfly type, presenting a deficiency of particles perpendicular to the magnetic field direction. Figure 7, which shows the H^+ distribution cuts for three instants (main plasmasphere and detached plasmasphere), confirms the bi-directional character of these distributions, showing that the particles in these detached plasma observations are trapped.

Figure 8 shows the time-of-flight spectra for three intervals, corresponding to these distribution cuts. As for the July 4, 2001 event, a persistent background due to penetrating

particles from the radiation belts is present in the first spectrum, obtained in the main plasmasphere. For the two following spectra, however, corresponding to the detached plasmasphere observations in the outbound leg of the orbit, the background disappears. These spectra show clearly the absence of O^+ ions. All spectra show the characteristic picks of H^+ and He^+.

The moments of the ion distribution functions of H^+, calculated in the ~0.7 eV/q to 25 eV/q energy range (with respect to spacecraft potential), are shown in Figure 9. The density values measured during the detached plasmasphere observations are by about an order of magnitude smaller than the ones measured in the main plasmasphere, consistent with the substantial density reduction for the detached plasma shells predicted by the peeling-off models [*Lemaire,* 2001]. The H^+ velocities measured here show a clear Vx > 0 and a Vy > 0 component in the main plasmasphere (~11 – 12 UT), corresponding to a corotating plasma (spacecraft position at 08:45 MLT). For the detached plasmasphere observations, however, around 13:30 UT, the velocities measured are dominated by Vy < 0 and Vz > 0 showing a strong outward expansion of the plasma tube. This expansion velocity increases as a function of the L-shell value: the spacecraft gets from L ≈ 50 at 13:22 UT to L ≈ 110 at 13:36 UT, on high-latitude lines, and the measured expansion velocity goes from ~3 km s^{-1} to ~10 km s^{-1} in that interval.

3.3 Detached Plasmasphere and Upwelling Ions Observations:

12 November 2001 Event

Figure 10 shows a crossing of the plasmasphere by Cluster sc 1 and 3, in the early morning sector (07:50 MLT), during quiet magnetospheric conditions (Kp = 0+, very quiet AE). Both spacecraft were in the RPA mode. Cluster sc 3 was lagging on its orbit, with respect to the other spacecraft, which explains why it crossed the plasmasphere about 30

minutes later. Sc 1 crossed the plasmaspheric main ion population between ~08:22 UT (L ≈ 5.3) and ~09:42 UT (L ≈ 6.3).

Around 07:00 UT (L ≈ 20), before the entry in the main plasmasphere, there appears in the energy-time spectrograms what looks as detached plasma of lower density. A similar observation appears also after the exit from the plasmasphere, at around 10:20 UT (L ≈ 11.7). An examination of the pitch-angle distributions (two middle panels in Figure 10) however shows that these two observations correspond to particle populations of very different characteristics. The observation around 07:00 UT, in the southern hemisphere (inbound leg), shows a very strong anisotropy, and is dominated by particles with pitch angles close to 0°. These are upwelling H^+ and O^+ ions, escaping from the ionosphere along the magnetic field lines [*Moore et al.,* 1986; *Chappell et al.,* 1987; *Sauvaud et al.*, 2004]. Although they are observed at low-energies, it is clear from the spectrograms that the population should also extend at energies above the RPA upper limit (25 eV/q).

The observation around 10:20 UT, on the contrary, at the outbound leg, is symmetric with respect to the magnetic field, and it corresponds to a trapped H^+ population. Contrary to the first one, this second observation corresponds thus to a detached plasmasphere.

Figure 11, which shows the H^+ and O^+ distribution cuts for three instants, confirms the observation of escaping H^+ and O^+ ions at ~07 UT. Their strong anisotropy contrasts with the bi-directional distributions detected later in the main plasmasphere and in the detached plasma event at the outbound leg.

Figure 12 shows the time-of-flight spectra for three intervals, corresponding to these distribution cuts. As for the July 4, 2001 event, a persistent background due to penetrating particles from the radiation belts is present in the second spectrum, obtained in the main plasmasphere. In the other spectra, however, corresponding to the upwelling ion observation

(upper panel) and to the detached plasmasphere observation (lower panel), there is no background. The first spectrum shows clearly the presence of O^+ ions, and even of O^{++} ions in this escaping population [*Truhlík*, 1997; *Wilber et al.,* 2003], in addition to the H^+ and He^+ ions. As shown in Figure 13, these upwelling ions are observed on auroral field lines. The spectrum in the bottom panel of Figure 12, however, shows the absence of ions heavier than He^+ in the detached plasmasphere.

3.4 Cluster Multi-Spacecraft Plasmasphere Observations: 17 February 2002 Event

In the first six months of 2002 the Cluster inter-spacecraft separation was reduced so as to obtain a regular tetrahedron of a 100 km characteristic size when traversing the cusp. This resulted in an elongated tetrahedron, of ~70 km width and ~240 km height mainly along the GSE z-axis, when crossing perigee.

Figure 14 shows a crossing of the plasmasphere by Cluster sc 1, 3 and 4, in the night sector (00:45 MLT), during moderately disturbed magnetospheric conditions (Kp = 2, AE ≈ 200 nT). Sc 1 and 3 were in the main plasmasphere between ~21:32 UT (L ≈ 4.3) and ~22:02 UT (L ≈ 4.2). Sc 4, however, did not at all detect the main plasmasphere, but only a low-density cold plasma, revealing the close presence of the plasmapause and the associated density gradient. The separation between sc 3 and sc 4, projected in the equatorial plane, was only 65 km. This gives a measure of the density gradients in the vicinity of the plasmapause, the density measured by sc 4 being lower by a factor of the order of 50-100 with respect to the one measured by sc 3. Note that the H^+ gyroradius at this region, for 2 eV plasmaspheric ions, is 0.6 km, i.e. consistent with the density gradients observed.

This localisation of the plasmapause, between the closely spaced Cluster spacecraft, allows to compare the observation with model predictions. The interchange instability numerical model for the plasmapause deformations [*Pierrard and Lemaire,* 2004] was used

here to simulate the February 17, 2002 event. This model uses as input an empirical Kp-dependent equatorial electric field model [*McIlwain,* 1986], and it determines, using kinetic simulations, the plasmapause position as the location where plasma interchange peels off the plasmasphere, i.e., where and when the magnetospheric convection velocity is enhanced at the onset of substorms [*Lemaire,* 1974, 2001]. According to this physical mechanism, the plasmapause is formed in the post-midnight MLT sector where and when the field-aligned component of the centrifugal pseudo-force overcomes that of the gravitational force.

The simulation results appear in Figure 15, bottom panel (equatorial plane). The blue dot corresponds to the Cluster spacecraft position (sc 1, 3 and 4), which appear as a single dot due to their close spacing: less than 100 km. It appears clearly that the spacecraft are almost at the edge of a plasmapause bulge, formed by plasma brought by interchange instability, explaining why only some of the spacecraft (1 and 3) got into the plasmasphere.

The February 17, 2002 plasmasphere observation included also an eclipse, which for example for sc 3 was between 21:46 UT and 22:09 UT (cf. Figure 16). The suppression of photoelectron production allows to evaluate the change in the spacecraft potential. The entrance in the plasmasphere (for sc1 and 3) is well before the start of the eclipse, and the exit from the plasmasphere (for sc1 and 3) is during the eclipse. The depth of the eclipse is almost the same for all sc. The only effect of the eclipse on the low-energy ions, detected by CIS-RPA, is a slight enhancement of the detected ion fluxes, and an increase in their energy by 1-2 eV, due to a more negative spacecraft potential by 1-2 V. This is compatible with the spacecraft potential measurements by the EFW electric field experiment onboard Cluster [*Gustafsson et al.,* 2001]. In the low-density magnetospheric lobes, however, the spacecraft potential can become positive by several Volts or even tens of Volts, unless the ASPOC ion emitter [*Torkar et al.,* 2001], used for the spacecraft active potential control, is operating.

At the outbound leg, around 01:00 UT (February 18, 2002) sc 4 detected three successive spikes of low-energy H^+ ions. As the pitch-angle distributions of these ions show (bottom panel of Figure 14), these are upwelling ions escaping from the ionosphere along the magnetic field lines. Their composition included only H^+ and He^+, and no O^+, as can be seen in the time-of-flight spectrum of Figure 17. It should be noted that the ASPOC ion emitter was operating, on sc 4, during this interval.

3.5 Cluster and Image Correlated Plasmasphere Observations: 9 August 2001 Event

On August 9, 2001, the Cluster spacecraft went through perigee in the noon sector (13:30 MLT), during the onset of a negative magnetic bay in the auroral zone (max AE = 500 nT, cf. Figure 18, Kp = 2), following a long period of quiet conditions (Kp = 1 for several hours). Sc 3 was in the plasmasphere between ~04:50 UT ($L \approx 4.4$) and ~05:50 UT ($L \approx 5.3$). Sc 1, however, did not at all detect the main plasmasphere, and the only signature in the particle data is some background from the radiation belts, also seen by sc 3 (Figure 19). It should be noted that sc 1 was leading on the orbit by 45 minutes: sc 1 went through perigee at 04:18 UT and sc 3 at 05:03 UT. The sc 3 orbit got also deeper into the inner magnetosphere, with a minimum L-shell value of 4.2, versus 4.3 minimum L for sc 1.

In order to interpret the difference in observations between these two Cluster spacecraft (the only ones operating in the RPA mode during this event), and deduce whether it was due to spatial effects (plasmapause situated between the trajectories of sc 1 and sc 3), or due to temporal effects (boundary motion), we examined the plasmaspheric images provided by the EUV experiment onboard the Image spacecraft [*Sandel et al.;* 2000].

Figure 20 shows a time series of three EUV images of the plasmasphere, projected in the magnetic equatorial plane. The reddish haze around the Earth is EUV-observed 30.4 nm emissions from He^+ (see figure caption for details). In each image, the Cluster sc 1 and sc 3

orbits (in blue and green respectively) are also mapped. The bottom panel of each image shows radial slices of the normalized EUV intensity. The first of the images in this time series is close to the Cluster sc 1 perigee pass (no plasmasphere detected in-situ by this spacecraft) and the second one is during the plasmaspheric observation by sc 3.

What appears in these images is a very diffuse plasmasphere, with a gradual fall-off of the plasma density and no clear plasmapause boundary, and also a lot of azimuthal variation. This resulted from the extended period of relatively quiet geomagnetic conditions, preceding the observations. It is possible, however, to define an ad-hoc plasmapause as where there is a gradient in intensity that passes through 100 or so [*Goldstein et al.,* 2003b].

The above definition of an ad-hoc plasmapause has been used to produce the white dotted line plots in the two panels of Figure 21, which show the intensity of the EUV 30.4 nm emissions at 13.5 MLT, as a function of UT and L. The projected sc 1 or sc 3 orbit is indicated with the blue or green curve, respectively, in the two panels.

These panels show a temporal dependence of the radial extent of the plasmasphere at 13.5 MLT. This is most clearly seen by looking for the bright (orange-yellow) region. The edge of this region starts at about L = 2.2 at 03:00 UT, and moves upward to about L = 2.8 by 05:45 UT. This bright orange-yellow region is the densest part of the plasmasphere. It is possible also to follow the red-orange (less dense) parts and see that they too move outward. The ad-hoc plasmapause moves outward between 04:30 and 05:45 UT as well. Sc 1 goes through 13.5 MLT when the ad-hoc plasmapause is just at about L = 4.2, just skimming above it. Sc 3 passes through 13.5 MLT when the ad-hoc plasmapause (at this MLT) has moved outward to L ≈ 4.8, passing well inside of it. This is consistent with the in-situ observation of the plasmasphere by sc 3, and the absence of plasmasphere detection by sc 1 (cf. Figure 19).

The outward motion of the plasmapause at 13.5 MLT, between the perigees of sc 1 and sc 3, is not a result of dynamic expansion of the global plasmapause. It results rather from the fact that the radial density profile of the plasmasphere varies with MLT, and a more extended radial profile "rotated" into 13.5 MLT in between the sc 1 and sc 3 perigees, due to the plasmasphere co-rotation with the Earth. Because there is so much azimuthal structure in the plasma density, this caused a slightly larger radial extent of the dense plasma to rotate into 13.5 MLT.

The interchange instability numerical model for the plasmapause deformations [*Pierrard and Lemaire,* 2004] was also used here to simulate this correlated Cluster – Image observation of the plasmasphere. Figure 22 shows the simulation results for the plasmapause geometry, for 04:21 UT (close to the Cluster sc 1 perigee pass) and for 05:43 UT (during the plasmaspheric observation by sc 3). The azimuthal structure in the "plasmapause" position is very clear. Since this is an event following an extended period of low – Kp, the model gives also a plasmapause position extending between 4 and 5 R_E. The blue dot, superposed on these simulations, corresponds to the Cluster sc 1position, and the green dot to sc 3.

In the 04:21 UT simulation results sc 3 is well outside the plasmasphere. Sc 1, however, appears as being situated within the plasmasphere, which is contrary to the Cluster and to the Image observations. To explain this we should take into account the fact that the only input parameter to the simulation is Kp, which is a 3-hour index. There is thus an uncertainty in the rotation phase of the plasmapause by about 1 - 2 hours. Introducing a phase delay of 2 hours in the plasmapause rotation is equivalent to rotating the spacecraft projected position, on the simulation results, by adding 2 hours in its MLT. This shifted azimuthal spacecraft position of sc 1 appears in the 04:21 UT simulation, Figure 22, as a red dot which now is very close to the boundary. Given the diffuse nature of the "plasmapause", for this

event, this is consistent with the Cluster and Image observations, showing sc 1 skimming just above it.

The same 2 hours phase delay in the plasmapause rotation was also applied to the 05:43 UT simulation results. The azimuthal position of sc 3, who was observing the plasmasphere, was shifted by adding 2 hours in its MLT (red dot). Sc 3 appears then well inside a bulge in the plasmasphere, consistently with the Cluster and Image observations.

3.6 Plasmaspause position: Statistical Analysis

Using the CIS-RPA data, a statistical analysis was performed of the observed plasmapause positions, for the period July 2001 – March 2003. The results appear in Figure 23, in an L - MLT azimuthal plot. Black corresponds to the Kp ≤ 1 events, blue to 1 < Kp < 3, and red to Kp ≥ 3. These results show the plasmasphere slightly more compressed in the night sector and extended outwards in the noon sector, consistently with the Image-EUV observations [*Sandel et al.,* 2003], and with the plasmapause observations by the Whisper resonance sounder experiment onboard Cluster [*Darouzet et al.,* 2003]. The plasmasphere erosion during high Kp activity appears as reduced L-shell values of the observed plasmapause positions.

Our results also show the characteristic "shoulder" in the 6 – 8 MLT sector (observations in the upper/upper-left part of Figure 23), which is an asymmetric bulge in the plasmapause and was seen for the first time in the EUV images [*Burch et al.,* 2001]. This is more clearly seen in Figure 24, which shows the average L-shell values of the plasmapause as a function of MLT (one average per MLT-hour). The formation in the afternoon-dusk sector of the plasmaspheric tail, or drainage plume [*Carpenter,* 1983; *Lemaire,* 2000; *Sandel et al.,* 2003], is another feature that appears also statistically in Figure 24. It should be noted,

however, that our observations do not allow to evaluate the full spatial extent of these structures, due to the limitations introduced by the Cluster spacecraft orbit (sampling effect).

The observations by CIS-RPA of low-energy O^+ ions, for the period July 2001 - March 2003, in an L – MLT azimuthal plot, are shown in Figure 25. All of these observations are outside of the main plasmasphere, and most of them correspond to upwelling ions, escaping from the ionosphere along the magnetic field lines (cf. November 12, 2001 event). For a few of these events, however, the O^+ distributions are bi-directional, indicating detached plasma, originating from deeper in the plasmasphere, and having an outwards expansion velocity. This was for example the case during the October 2, 2001 event, around 23:20 UT, when sc 4 observed in the morning sector (09:45 MLT, $L \approx 6$) detached plasma, including O^+ ions, presenting symmetric bi-directional pitch-angle distributions and having an outwards expansion velocity of ~3 km/s (data not shown). We should notice, however, that O^+ ions were never observed in the main plasmasphere, at the Cluster altitudes (perigee at about 4 R_E).

4. DISCUSSION AND CONCLUSIONS

We have analyzed some typical events, representative of the ionic structures observed in or close to the outer plasmasphere by the CIS experiment onboard the Cluster spacecraft [*Rème et al.,* 2001]. A statistical study has been also performed on these observations. Our data allow to reconstruct statistically the plasmapause morphology and dynamics, but they also reveal new and interesting features. From our analysis, we can conclude that:

- The H^+ and He^+ ions present mostly similar density profiles, with the He^+ densities being lower by a factor of ~15.

- O^+ ions, however, are not observed as part of the main plasmaspheric population at the Cluster orbit altitudes ($R \geq 4$ R_E).
- Detached plasmasphere events, that are observed by CIS during some of the passes at about 0.5 to 1 R_E outside of the plasmapause, are also present. The symmetric bi-directional pitch-angle distribution functions of these detached plasmaspheric populations allow us to distinguish them from upwelling ion populations.
- The density values measured during the detached plasmasphere observations are by about an order of magnitude lower than the ones measured in the main plasmasphere, consistently with the substantial density reduction for the detached plasma shells predicted by the peeling-off models [*Lemaire,* 2001].
- The plasmasphere co-rotation with the Earth is observed in the ion distribution functions, acquired within the main plasmasphere. In the detached plasmasphere observations, however, the plasma is not corotating, but has a strong outwards expansion velocity, which is increasing as a function of the L-shell value.
- Low-energy ($E < 25$ eV) O^+ is observed only as upwelling ions, escaping from the ionosphere along auroral field lines. O^{++} can be also observed in these upwelling ion populations. Furthermore, in a few cases low-energy O^+ ions have been observed as detached plasma, presenting trapped bi-directional pitch-angle distributions and having an outwards expansion velocity.
- The CIS-RPA observations of the plasmapause position have been simulated with an interchange instability numerical model for the plasmapause deformations [*Pierrard and Lemaire,* 2004], that uses as input an empirical Kp-dependent equatorial electric field model [*McIlwain,* 1986]. The numerical model reproduces in a very satisfactory way the CIS observations.

- The CIS local ion measurements have been also correlated with global images of the plasmasphere, obtained by the EUV instrument onboard Image [*Sandel et al.,* 2000], for an event where the Cluster spacecraft were within the field-of-view of EUV. The EUV images show, for this event, that the difference observed between two Cluster spacecraft was temporal (boundary motion): the radial density profile of the plasmasphere varies with MLT, and a more extended radial profile "rotated" into between the two Cluster spacecraft perigee passes. They thus show the necessity for correlating local measurements with global images, and the complementarity of the two approaches; local measurements giving the "ground truth" (including plasma composition, distribution functions etc.) and global images allowing to put local measurements into a global context, and to deconvolve spatial from temporal effects.

Acknowledgments

The Kp index was provided by the GeoForschungsZentrum, Potsdam, and the AE index by the World Data Center for Geomagnetism, Kyoto.

REFERENCES

Balogh, A., C. M. Carr, M. H. Acuña, M. W. Dunlop, T. J. Beek, P. Brown, K.-H. Fornaçon, E. Georgescu, K.-H. Glassmeier, J. Harris, G. Musmann, T. Oddy, K. Schwingenschuh, The Cluster Magnetic Field Investigation: overview of in-flight performance and initial results*, Ann. Geophys*., 19, 1207, 2001.

Bezrukikh, V. V., M. I. Verigin, G. A. Kotova, L. A. Lezhen, Yu. I. Venediktov, J. Lemaire, Dynamics of the plasmasphere and plasmapause under the action of geomagnetic storms, *J. Atmosph. Sol.-Terr. Phys., 63,* 1179-1184, 2001.

Burch, J. L., (Ed), *The IMAGE Mission*, Kluwer Acad., Norwell, Mass., 2000 (Reprinted from Space Sci. Rev., 91), 2000.

Burch, J. L., D. G. Mitchell, B. R. Sandel, P. C. Brandt, M. Wüest, Global dynamics of the plasmasphere and ring current during magnetic storms, *Geophys. Res. Lett., 28,* 6, 1159-1162, 2001.

Carpenter, D. L., Some aspects of plasmapause probing by whistlers, *Radio Sci., 18,* 917-925, 1983.

Chappell, C. R., T. E. Moore, and J. H. Waite, Jr., The ionosphere as a fully adequate source of plasma for the earth's magnetosphere, *J. Geophys. Res., 92,* 5896-5910, 1987.

Comfort, R. H., Thermal structure of the plasmasphere, *Adv. Space Res., 17,* (10) 175-(10) 184, 1996.

Craven, P. D., D. L. Gallagher, and R. H. Comfort, Relative concentration of He^+ in the inner magnetosphere as observed by the DE1 retarding ion mass spectrometer, *J. Geophys. Res., 102,* 2279-2289, 1997.

Darrouzet, F., P. M. E. Décréau, J. Lemaire, A. Masson, E. Le Guirriec, J. G. Trotignon, J. L. Rauch, P. Canu, F. Sedgemore, and M. André, Density irregularities at the plasmapause: Cluster observations, *EGS - AGU - EUG Joint Assembly,* Nice, France, 6-11 April 2003.

Décréau, P. M. E., P. Fergeau, V. Krasnoselskikh, E. LeGuirriec, M. Lévêque, Ph. Martin, O. Randriamboarison, J. L. Rauch, F. X. Sené, H. C. Séran, J. G. Trotignon, P. Canu, N. Cornilleau, H. de Féraudy, H. Alleyne, K. Yearby, P. B. Mögensen, G. Gustafsson, M. André, D. C. Gurnett, F. Darrouzet, J. Lemaire, C. C. Harvey, P. Travnicek, and Whisper experimenters, Early results from the Whisper instrument on Cluster: an overview, *Ann. Geophys., 19,* 1241–1258, 2001.

Escoubet,C. P., M. Fehringer, and M. Goldstein, The Cluster mission, *Ann. Geophys., 19,* 1197-1200, 2001.

Goldstein, J., B. R. Sandel, M. R. Hairston, and P. H. Reiff, Control of plasmaspheric dynamics by both convection and sub-auroral polarization stream, *Geophys. Res. Lett., 30,* 24, 2243, doi: 10.1029/2003GL018390, 2003a.

Goldstein J., M. Spasojevic´, P. H. Reiff, B. R. Sandel, W. T. Forrester, D. L. Gallagher, and B. W. Reinisch, Identifying the plasmapause in IMAGE EUV data using IMAGE RPI in situ steep density gradients, *J. Geophys. Res., 108,* 1147, doi: 10.1029/2002JA009475, 2003b.

Gustafsson, G., M. André, T. Carozzi, A. I. Eriksson, C.-G. Fälthammar, R. Grard, G. Holmgren, J. A. Holtet, N. Ivchenko, T. Karlsson, Y. Khotyaintsev, S. Klimov, H. Laakso, P.-A. Lindqvist, B. Lybekk, G. Marklund, F. Mozer, K. Mursula, A. Pedersen, B. Popielawska, S. Savin, K. Stasiewicz, P. Tanskanen, A. Vaivads, and

J-E. Wahlund, First results of electric field and density observations by Cluster EFW based on initial months of operation, *Ann. Geophys*., *19*, 1219 - 1240, 2001.

Lemaire, J., The "Roche-limit" of ionospheric plasma and the formation of the plasmapause, *Planet. Space Sci., 22,* 757-766, 1974.

Lemaire, J. F., The formation of plasmaspheric tails, *Phys. Chem. Earth, 25,* 9-17, 2000.

Lemaire, J. F., The formation of the light-ion trough and peeling off the plasmasphere, *J. Atmosph. Sol.-Terr. Phys., 63,* 1285-1291, 2001.

Lemaire, J. F., and K. I. Gringauz, with contributions from D. L. Carpenter and V. Bassolo, *The Earth's Plasmasphere,* Cambridge University Press, Cambridge, 1998.

McIlwain, C. E., A Kp dependent equatorial electric field model, The Physics of Thermal plasma in the magnetosphere, *Adv. Space Res., 6(3),* 187–197, 1986.

Moore, T. E., M. Lockwood, M. O. Chandler, J. H. Waite, Jr., C. R. Chappell, A. Persoon, and M. Sugiura, Upwelling O^+ ion source characteristics, *J. Geophys. Res., 91,* 7019-7031, 1986.

Moullard, O., A. Masson, H. Laakso, M. Parrot, P. Décréau, O. Santolik, and M. André, Density modulated whistler mode emissions observed near the plasmapause, *Geophys. Res. Lett., 29,* 20, 1975, doi: 10.1029/2002GL015101, 2002.

Pierrard, V., and J. F. Lemaire, Development of shoulders and plumes in the frame of the interchange instability mechanism for plasmapause formation, *Geophys. Res. Lett., 31,* L05809, doi: 10.1029/2003GL018919, 2004.

Rème, H., C. Aoustin, J. M. Bosqued, I. Dandouras, B. Lavraud, J. A. Sauvaud, A. Barthe, J. Bouyssou, Th. Camus, O. Coeur-Joly, A. Cros, J. Cuvilo, F. Ducay, Y. Garbarowitz, J. L. Medale, E. Penou, H. Perrier, D. Romefort, J. Rouzaud, C. Vallat, D. Alcaydé,

C. Jacquey, C. Mazelle, C. dâUston, E. Möbius, L.M. Kistler, K. Crocker, M. Granoff, C. Mouikis, M. Popecki, M. Vosbury, B. Klecker, D. Hovestadt, H. Kucharek, E. Kuenneth, G. Paschmann, M. Scholer, N. Sckopke, E. Seidenschwang, C. W. Carlson, D. W. Curtis, C. Ingraham, R. P. Lin, J. P. McFadden, G. K. Parks, T. Phan, V. Formisano, E. Amata, M. B. Bavassano-Cattaneo, P. Baldetti, R. Bruno, G. Chionchio, A. Di Lellis, M.F. Marcucci, G. Pallocchia, A. Korth, P. W. Daly, B. Graeve, H. Rosenbauer, V. Vasyliunas, M. McCarthy, M. Wilber, L. Eliasson, R. Lundin, S. Olsen, E. G. Shelley, S. Fuselier, A. G. Ghielmetti, W. Lennartsson, C. P. Escoubet, H. Balsiger, R. Friedel, J-B. Cao, R. A. Kovrazhkin, I. Papamastorakis, R. Pellat, J. Scudder, and B. Sonnerup, First multispacecraft ion measurements in and near the earth's magnetosphere with the identical CLUSTER Ion Spectrometry (CIS) Experiment, *Ann. Geophys*., *19*, 1303-1354, 2001.

Sandel, B. R., A. L Broadfoot, C. C Curtis, R. A. King, T. C. Stone, R. H. Hill, J. Chen, O. H. W. Siegmund, R. Raffanti, D. D. Allred, R.S. Turley, and D.L. Gallagher, The extreme ultraviolet imager investigation for the IMAGE mission, *Space Science Reviews, 91,* 197–242, 2000.

Sandel, B. R., J. Goldstein, D. L. Gallagher, and M. Spasojevic´, Extreme ultraviolet imager observations of the structure and dynamics of the plasmasphere, *Space Sci. Rev., 109,* 25-46, 2003.

Sauvaud, J. A., P. Louarn, G. Fruit, H. Stenuit, C. Vallat, J. Dandouras, H. Rème, M. André, A. Balogh, M. Dunlop, L. Kistler, E. Möbius, C. Mouikis, B. Klecker, G. K. Parks, J. McFadden, C. Carlson, F. Marcucci, G. Pallocchia, R. Lundin, A. Korth, and M. McCarthy, Cases studies of the dynamics of ionospheric ions in the Earth's magnetotail, *J. Geophys. Res., 109,* A01212, 10.1029/2003JA009996, 2004.

Torkar, K., W. Riedler, C. P. Escoubet, M. Fehringer, R. Schmidt, R. J. L. Grard, H. Arends, F. Rüdenauer , W. Steiger, B. T. Narheim, K. Svenes, R. Torbert, M. André, A. Fazakerley, R. Goldstein, R. C. Olsen, A. Pedersen, E. Whipple, and H. Zhao, Active spacecraft potential control for Cluster – implementation and first results, *Ann. Geophys*., *19*, 1289 - 1302, 2001.

Truhlík, V., Theoretical interpretation of thermal O^{++} ions density enhancement in the midlatitude outer ionosphere, *Adv. Space Res., 20,* 3, 419-423, 1997.

Vallat, C., I. Dandouras, P. C:son Brandt, D. G. Mitchell, E. C. Roelof, R. deMajistre, H. Rème, J.-A. Sauvaud, L. Kistler, C. Mouikis, M. Dunlop, and A. Balogh, First comparisons of local ion measurements in the inner magnetosphere with ENA magnetospheric image inversions: Cluster-CIS and IMAGE-HENA observations, *J. Geophys. Res., 109,* A04213, 10.1029/2003JA010224, 2004.

Wilber, M.; G. Parks, H. Rème, L. Kistler, I. Dandouras, M. McCarthy, C. Carlson, J. McFadden, and J. A. Sauvaud, Results from initial Cluster/CIS survey of O^{++}, *EGS - AGU - EUG Joint Assembly,* Nice, France, 6-11 April 2003.

FIGURE CAPTIONS

Figure 1: CIS (Cluster) and EUV (Image) measurements comparison principle : the CIS local ion measurements are correlated with global images of the plasmasphere, obtained by the EUV instrument onboard Image, for an event where the Cluster spacecraft were within the field-of-view of EUV.

Figure 2: Cluster spacecraft 3 ion data for July 4, 2001. From top to bottom: HIA energy-time ion spectrogram (normal magnetospheric mode: 5 eV/q – 32 keV/q), in corrected-for-detection-efficiency counts per sec. (c/s) ; CODIF mode (in black: RPA mode until 16:00 UT); CODIF Energy-time ion spectrograms, separately for H^+, He^+, and O^+; spacecraft coordinates (GSE system) and geocentric distance, in R_E.

Figure 3: Cluster spacecraft 3 orbit (in red) for July 4, 2001, projected on the Tsyganenko 89 magnetic field model. Orbit Visualization Tool plot, courtesy of the OVT Team.

Figure 4: Time-of-flight spectrum for the ions detected by CODIF between 11:30 and 12:40 UT (Cluster sc 3, July 4, 2001). The abscissa axis is the time-of-flight channel number (inversely proportional to the ion velocity), and the ordinate axis is the number of particles in a given channel (with two different sampling laws above and below channel 31).

Figure 5a: Cluster sc 3 CODIF H^+ data for July 4, 2001. From top to bottom: Energy-time ion spectrogram and moments of the distribution functions (~0.7 eV/q to 25 eV/q energy range): density, velocity (in GSE coordinates), and parallel and perpendicular temperatures.

Figure 5b: Same as Figure 5a, but for He^+ ions.

Figure 6: Cluster sc 1, 3 and 4 H^+ and He^+ energy-time ion spectrograms, in corrected-for-detection-efficiency counts per sec., for October 31, 2001. All spacecraft in

RPA mode. Bottom panel: sc 4 pitch-angle distributions for H^+ ions (~0.7 eV/q to 25 eV/q energy range), in particle flux units (cm^{-2} sr^{-1} s^{-1} keV^{-1}).

Figure 7: H^+ distribution cuts in three perpendicular planes each, for the October 31, 2001 event, in GSE coordinates and in particle distribution units (phase-space density: sec^3 km^{-6}), for three instants: 11:27:04 UT (main plasmasphere), 12:26:03 UT (detached plasmasphere), and 13:25:01 UT (detached plasmasphere).

Figure 8: Time-of-flight spectra, same format as in Figure 4, for the ions detected by CODIF on sc 4 during the October 31, 2001 event, for three intervals: 11:10 – 11:50 UT (main plasmasphere), 12:20 – 12:35 UT (detached plasmasphere), and 13:24 – 13:36 UT (detached plasmasphere). These three intervals correspond to the distributions shown in Figure 7.

Figure 9: Cluster sc 4 CODIF H^+ data for October 31, 2001. From top to bottom: Energy-time ion spectrogram and moments of the distribution functions (~0.7 eV/q to 25 eV/q energy range): density, velocity (in GSE coordinates).

Figure 10: Cluster sc 1 and 3 H^+, He^+ and O^+ energy-time ion spectrograms, in corrected-for-detection-efficiency counts per sec., for November 12, 2001. Both spacecraft in RPA mode. Middle two panels show sc 1 pitch-angle distributions for H^+ and O^+ ions (~0.7 eV/q to 25 eV/q energy range), in particle flux units (cm^{-2} sr^{-1} s^{-1} keV^{-1}).

Figure 11: H^+ and O^+ distribution cuts in three perpendicular planes each, for the November 12, 2001 event, in GSE coordinates and in particle distribution units (phase-space density: sec^3 km^{-6}), for three instants: 07:04:10 UT (upwelling H^+ and O^+ ions), 09:02:14 UT (main plasmasphere), and 10:20:34 UT (detached plasmasphere).

Figure 12: Time-of-flight spectra, same format as in Figures 4 and 8, for the ions detected by CODIF on sc 1 during the November 12, 2001 event, for three intervals: 06:45 –

07:10 UT (upwelling ions), 08:50 – 09:20 UT (main plasmasphere), and 10:09 – 10:32 UT (detached plasmasphere). These three intervals correspond to the distributions shown in Figure 11.

Figure 13: Cluster sc 1 orbit (in black) for November 12, 2001, projected on the Tsyganenko 89 magnetic field model. Orbit Visualization Tool plot, courtesy of the OVT Team.

Figure 14: Cluster sc 1, 3 and 4 H^+, He^+ and O^+ energy-time ion spectrograms, in corrected-for-detection-efficiency counts per sec., for February 17, 2002. All spacecraft in RPA mode. Bottom panel: sc 4 pitch-angle distributions for H^+ ions (~0.7 eV/q to 25 eV/q energy range), in particle flux units (cm^{-2} sr^{-1} s^{-1} keV^{-1}).

Figure 15: Numerical simulation results of the plasmapause deformations, for February 17, 2002, using the interchange instability model. Upper panel: Kp index time history, used as input parameter for the simulation. Bottom panel: simulation results of the plasmapause deformations, in the equatorial plane. The blue dot corresponds to the Cluster spacecraft position (sc 1, 3 and 4), which appear as a single dot due to their close spacing.

Figure 16: Cluster sc 1, 3 and 4 H^+ energy-time ion spectrograms, for February 17, 2002. The bottom panel shows an indicator of the spacecraft penetration within the eclipse shadow cone.

Figure 17: Time-of-flight spectrum, same format as in Figure 4, for the upwelling ions detected by CODIF on sc 4 during the interval 00:44 – 01:02 UT on February 18, 2002.

Figure 18: AE index for August 9, 2001.

Figure 19: Cluster sc 1 and 3 H^+, He^+ and O^+ energy-time ion spectrograms, in corrected-for-detection-efficiency counts per sec., for August 9, 2001. Both spacecraft in RPA mode.

Figure 20: Series of three EUV images of the plasmasphere, for August 9, 2001. In each image the top panel shows the projection in the magnetic equatorial plane. The Earth is in the center, and the Sun direction is to the right. The reddish haze around the Earth is EUV-observed 30.4 nm emissions from He^+. The black regions mark the edges of the EUV field of view, distorted because the edges have been mapped to the equator. The blue and green lines are the Cluster sc 1 and 3 orbits (respectively), mapped to the equator. The dot shows where the satellite is at the given time. The bottom panel of each image shows radial slices through the EUV equatorial image, with the vertical axis being intensity (from 0-255) and the horizontal axis being L-shell. The blue curve is a radial intensity slice at the Cluster sc 1 perigee MLT and the green curve is for sc 3. (Sc 1 and sc 3 are at slightly different MLT, although rounded off to one decimal place they are both at 13.5 MLT). The vertical dotted lines mark the perigee L-shell of each spacecraft (blue for sc 1 and green for sc 3). The vertical solid lines show the instantaneous L-positions of each spacecraft.

Figure 21: Two panels of Image-EUV data (upper and lower, one for each Cluster spacecraft sc1 and sc3). In each panel the color corresponds to the intensity of the EUV 30.4 nm emissions at 13.5 MLT, as a function of UT and L. The projected sc 1 or sc 3 orbit is indicated with the blue or green curve, respectively. The ad-hoc plasmapause L-value (see texte) is the white dotted line. The intervals [2:59, 3:10, 3:51, 4:01, 4:11] correspond to high background noise.

Figure 22: Numerical simulation results of the plasmapause deformations, for August 9, 2001, using the interchange instability model. Upper panel: Kp index time history, used as input parameter for the simulation. Middle and bottom panel: simulation results of the plasmapause deformations, in the equatorial plane, at 04:21 UT and at 05:43 UT. The blue dot corresponds to the Cluster sc 1spacecraft position and the green to sc 3. The red corresponds

to the relative position of sc 1 (middle panel) and sc 3 (bottom panel), if a 2 hours delay is introduced in the plasmasphere rotation (see text).

Figure 23: Observed plasmapause positions, by the CIS experiment onboard Cluster, for the period July 2001 – March 2003, in an L - MLT azimuthal plot (local noon at left). Black corresponds to Kp ≤ 1 events, blue to 1 < Kp < 3, and red to Kp ≥ 3. The blue circle corresponds to L = 5.

Figure 24: Average plasmapause L-shell positions (all Kp), observed by CIS, as a function of MLT.

Figure 25: Observed low-energy O^+ ions by CIS-RPA, for the period July 2001 - March 2003, in an L – MLT azimuthal plot (local noon at left). The blue circles correspond to L = 3.5 and to L = 5.0.

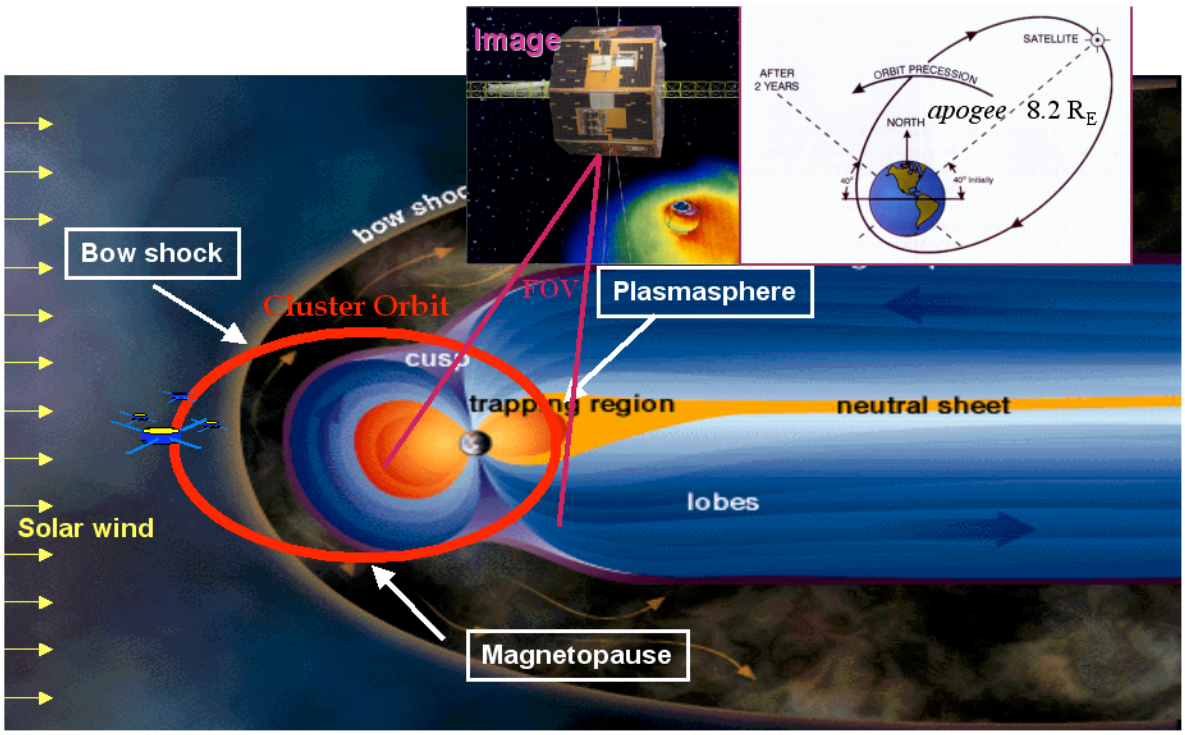
Image
SATELLITE
AFTER 2 YEARS
ORBIT PRECESSION
NORTH
apogee
8.2 R_E
Bow shock
Cluster Orbit
FOV
Plasmasphere
cusp
trapping region
neutral sheet
lobes
Solar wind
Magnetopause

Figure 1

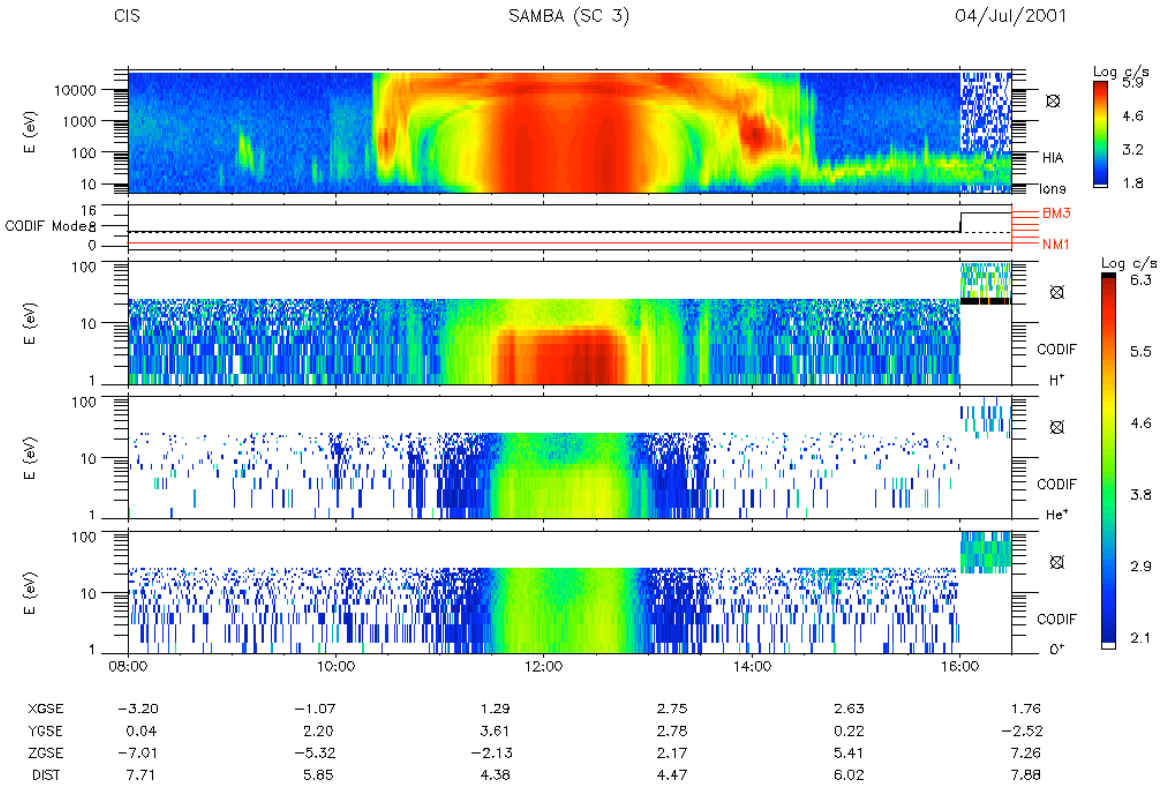
CIS
SAMBA (SC 3)
04/Jul/2001
E (eV)
10000
1000
100
10
HIA
Ions
Log c/s
5.9
4.6
3.2
1.8
CODIF Mode
16
8
0
BM3
NM1
100
10
1
CODIF
H+
He+
O+
Log c/s
6.3
5.5
4.6
3.8
2.9
2.1
08:00
10:00
12:00
14:00
16:00
XGSE −3.20 −1.07 1.29 2.75 2.63 1.76
YGSE 0.04 2.20 3.61 2.78 0.22 −2.52
ZGSE −7.01 −5.32 −2.13 2.17 5.41 7.26
DIST 7.71 5.85 4.38 4.47 6.02 7.88

Figure 2

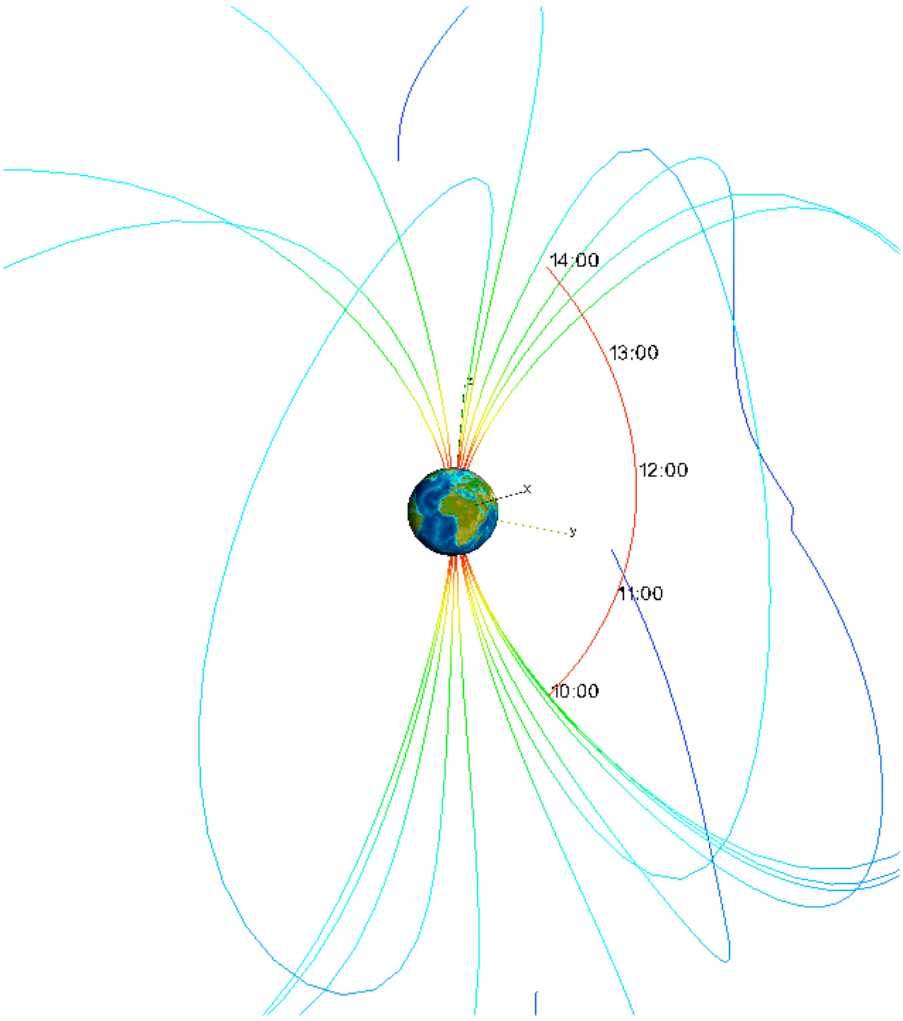

Figure 3

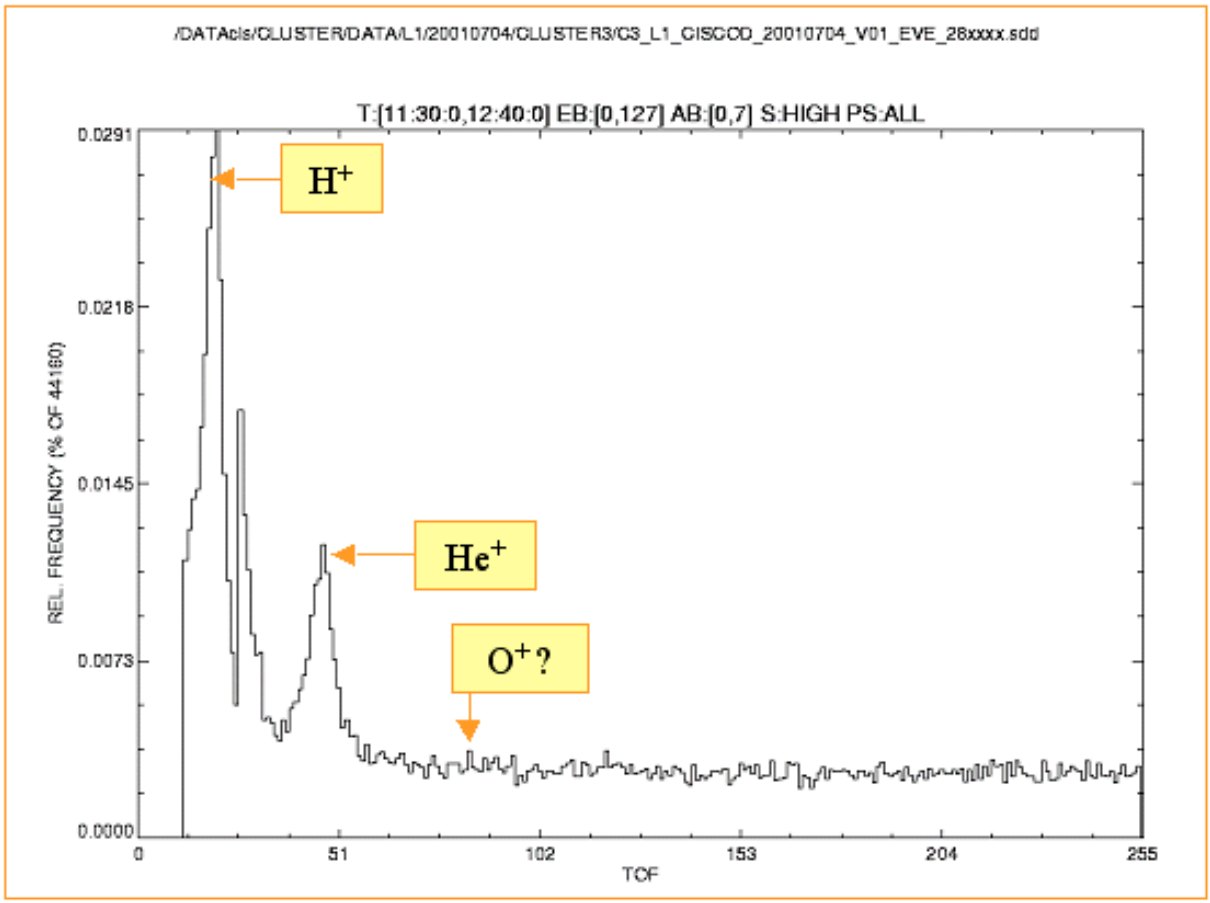
/DATAcls/CLUSTER/DATA/L1/20010704/CLUSTER3/C3_L1_CISCOD_20010704_V01_EVE_28xxxx.sdd
T:[11:30:0,12:40:0] EB:[0,127] AB:[0,7] S:HIGH PS:ALL
H+
He+
O+?
REL. FREQUENCY (% OF 44160)
0.0291
0.0218
0.0145
0.0073
0.0000
0
51
102
153
204
255
TOF

Figure 4

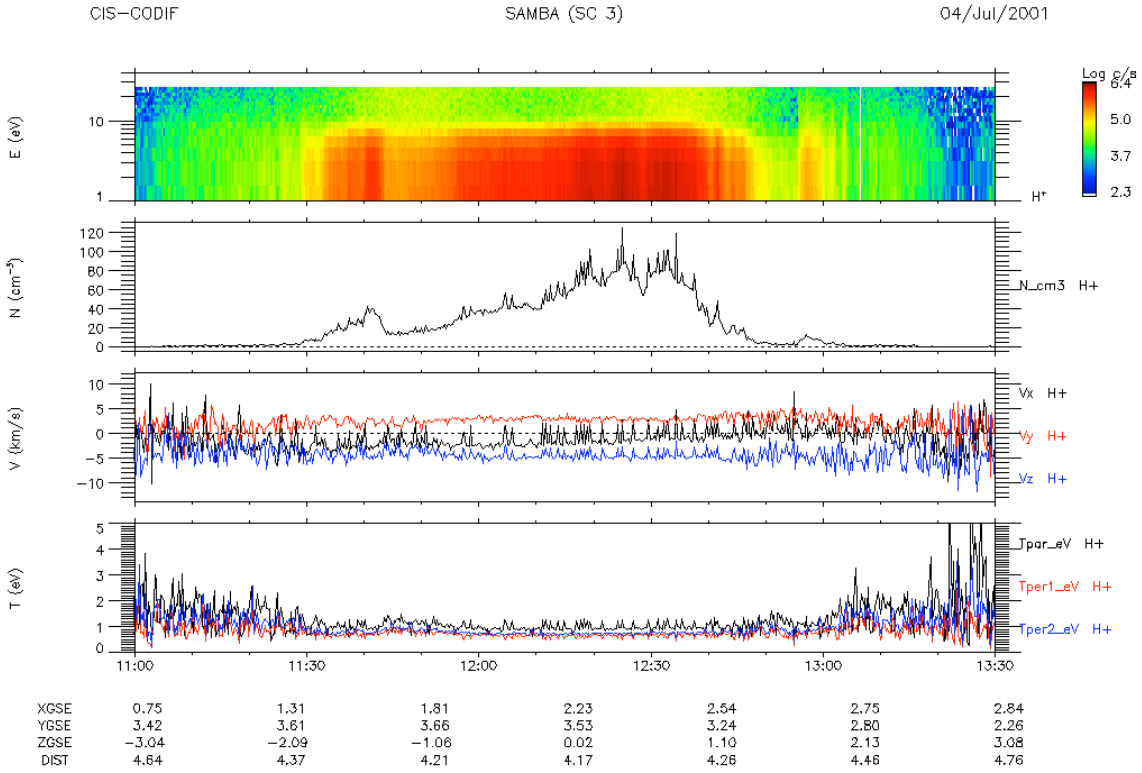

Figure 5a

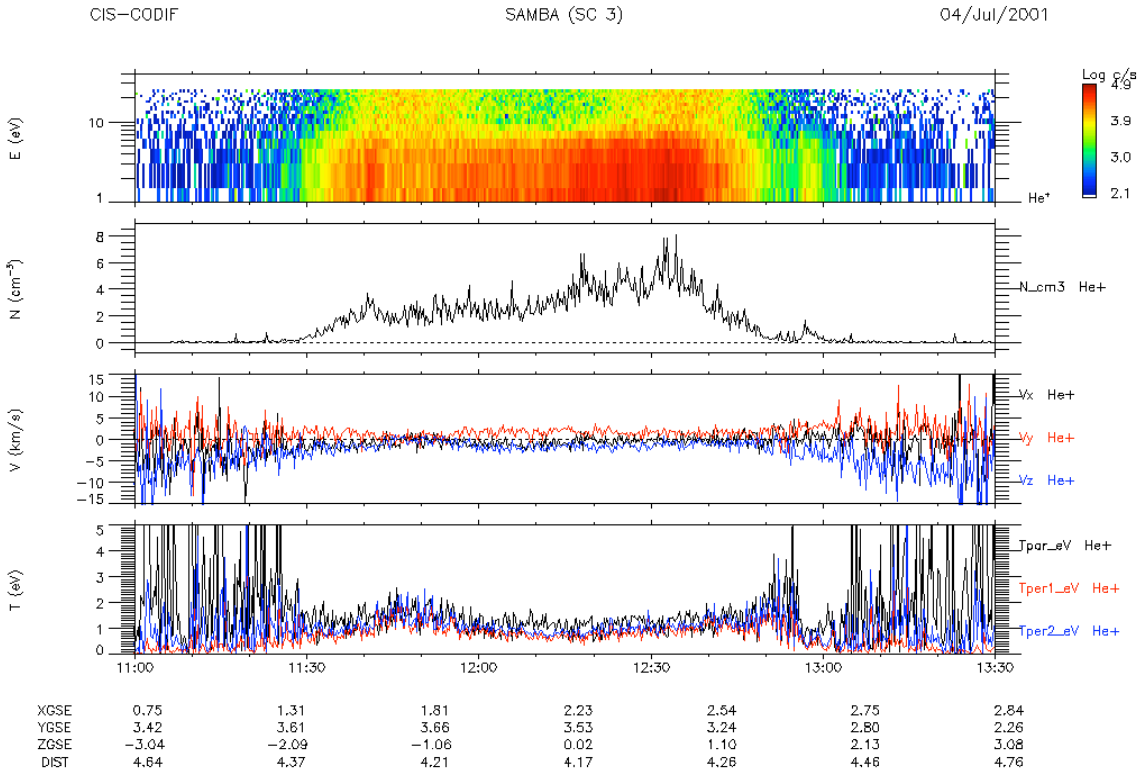

Figure 5b

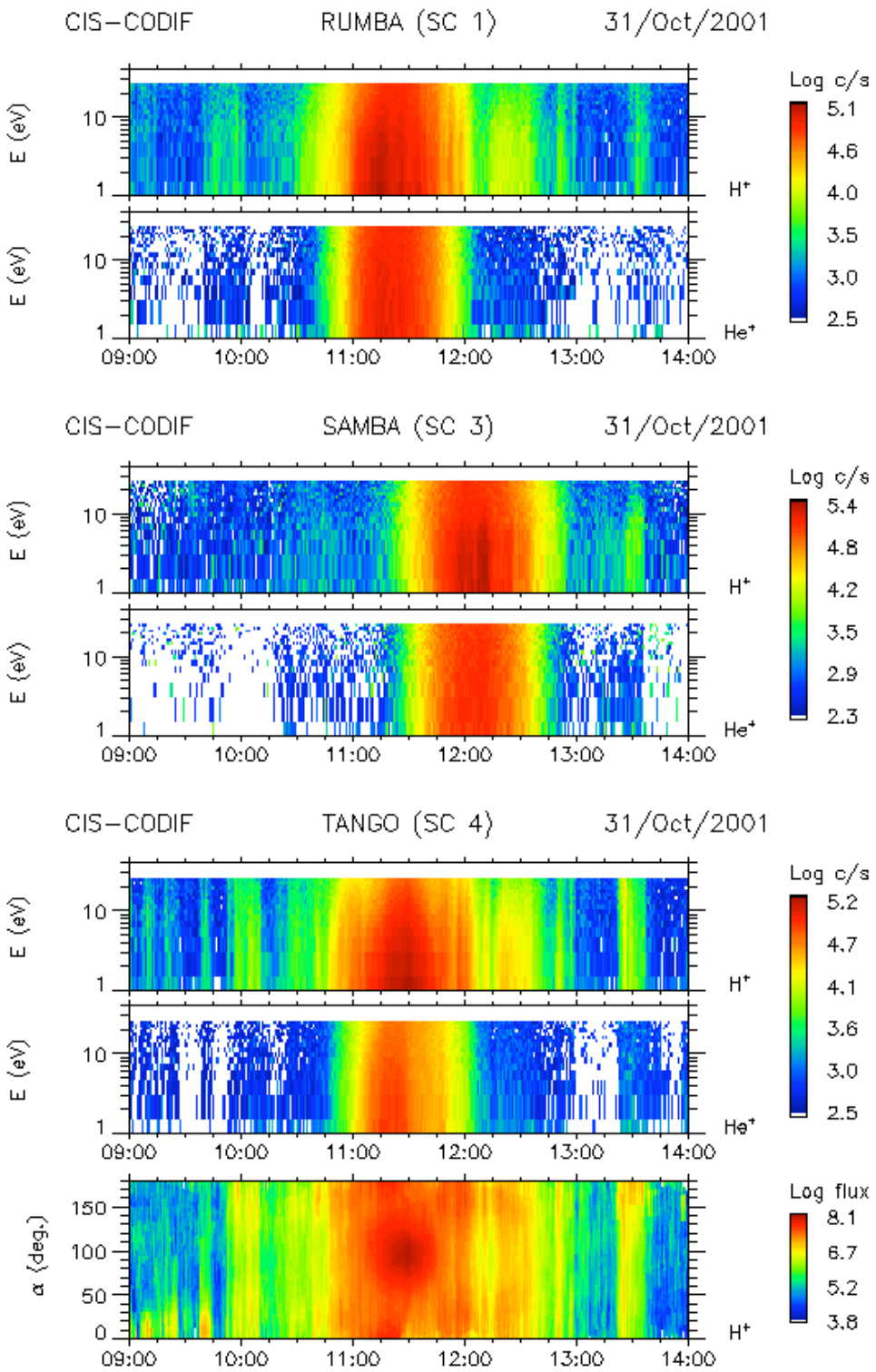
CIS–CODIF
RUMBA (SC 1)
31/Oct/2001
E (eV)
10
1
H+
He+
09:00
10:00
11:00
12:00
13:00
14:00
Log c/s
5.1
4.6
4.0
3.5
3.0
2.5
CIS–CODIF
SAMBA (SC 3)
31/Oct/2001
5.4
4.8
4.2
3.5
2.9
2.3
CIS–CODIF
TANGO (SC 4)
31/Oct/2001
5.2
4.7
4.1
3.6
3.0
2.5
α (deg.)
150
100
50
0
Log flux
8.1
6.7
5.2
3.8

Figure 6

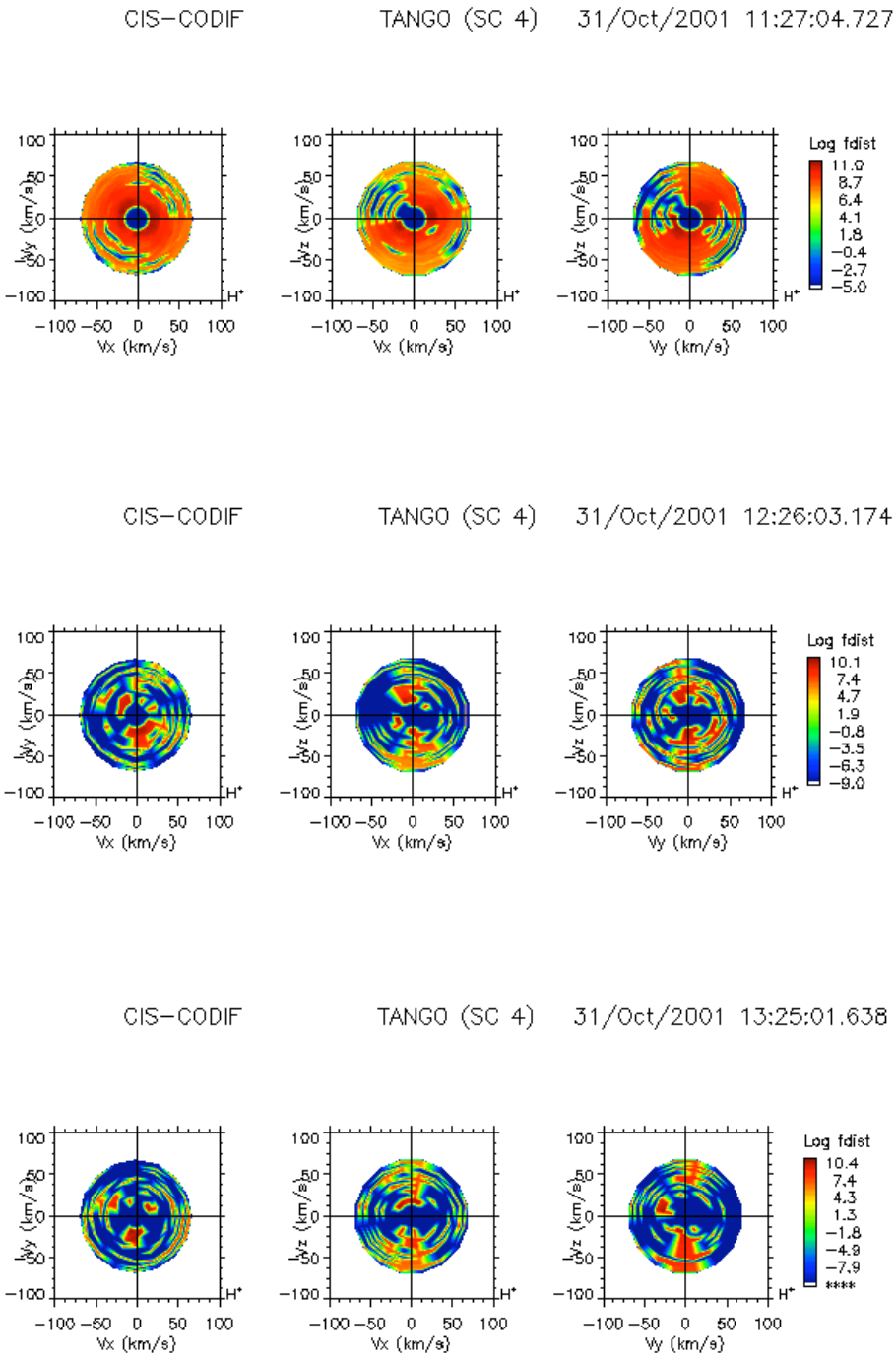
CIS-CODIF TANGO (SC 4) 31/Oct/2001 11:27:04.727
Log fdist
11.0
8.7
6.4
4.1
1.8
−0.4
−2.7
−5.0
Vx (km/s)
Vy (km/s)
Vz (km/s)
H+
CIS-CODIF TANGO (SC 4) 31/Oct/2001 12:26:03.174
Log fdist
10.1
7.4
4.7
1.9
−0.8
−3.5
−6.3
−9.0
CIS-CODIF TANGO (SC 4) 31/Oct/2001 13:25:01.638
Log fdist
10.4
7.4
4.3
1.3
−1.8
−4.9
−7.9
****

Figure 7

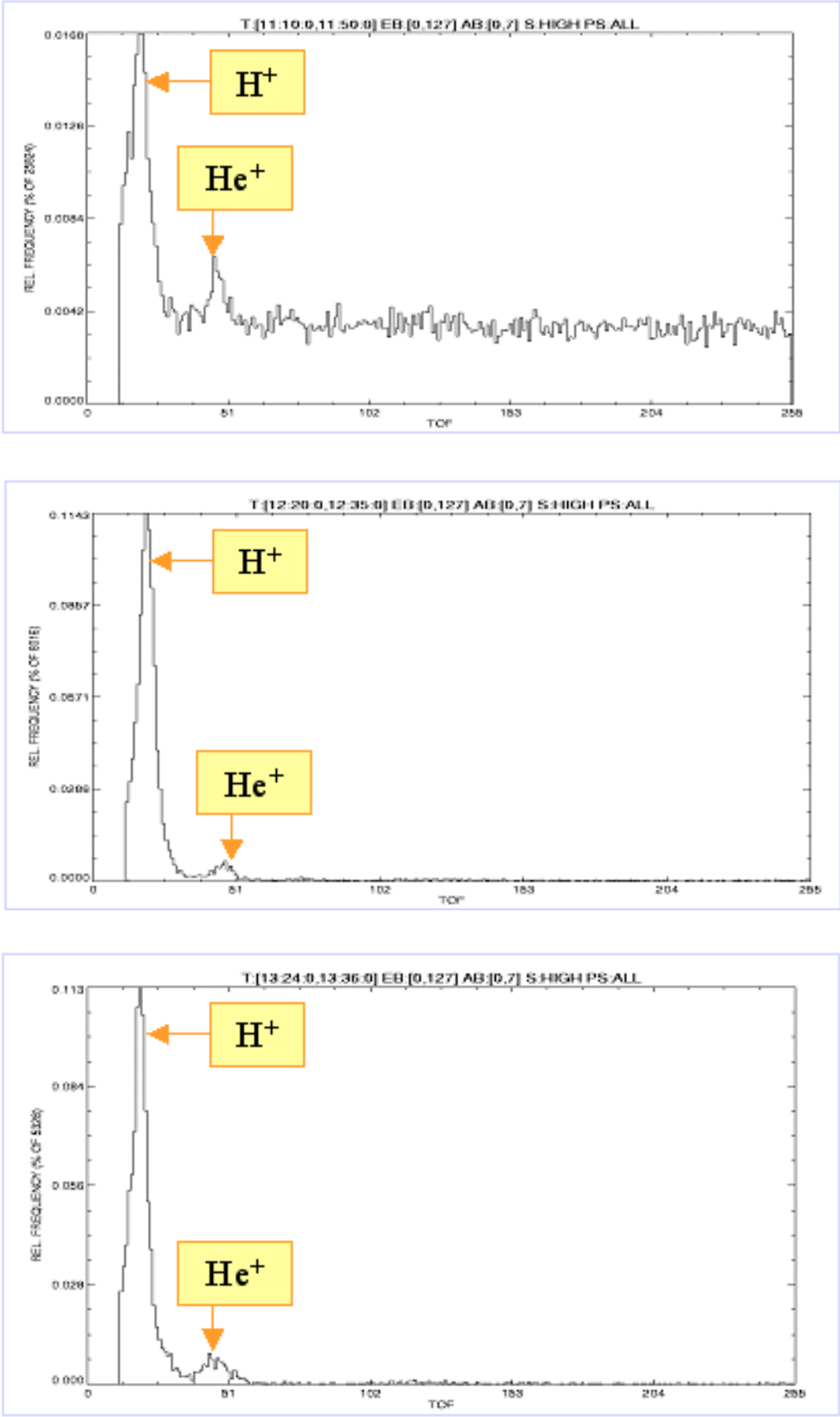
T:[11:10:0,11:50:0] EB:[0,127] AB:[0,7] S:HIGH PS:ALL
H+
He+
REL FREQUENCY (% OF 2924)
0.0168
0.0126
0.0084
0.0042
0.0000
0
51
102
153
204
255
TOF
T:[12:20:0,12:35:0] EB:[0,127] AB:[0,7] S:HIGH PS:ALL
H+
He+
REL FREQUENCY (% OF 6816)
0.1142
0.0857
0.0571
0.0286
0.0000
0
51
102
153
204
255
TOF
T:[13:24:0,13:36:0] EB:[0,127] AB:[0,7] S:HIGH PS:ALL
H+
He+
REL FREQUENCY (% OF 5388)
0.113
0.084
0.056
0.028
0.000
0
51
102
153
204
255
TOF

Figure 8

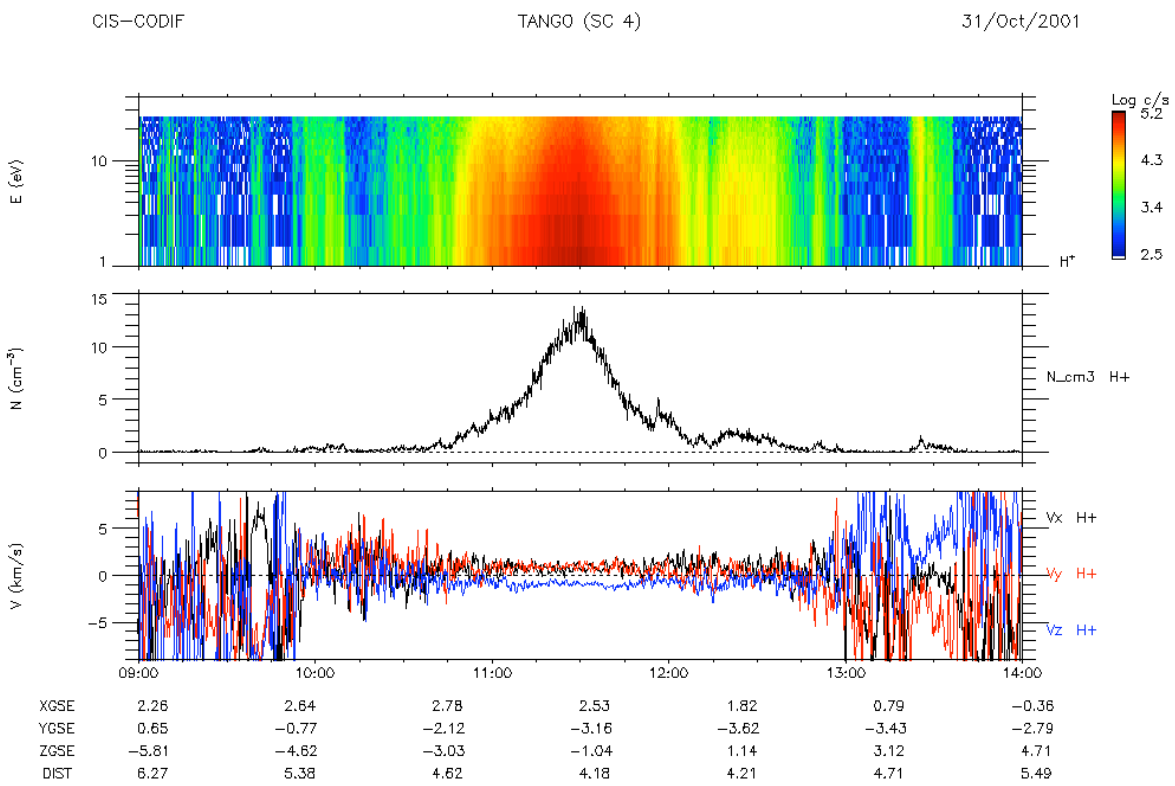
CIS–CODIF
TANGO (SC 4)
31/Oct/2001
E (ev)
10
1
H+
Log c/s
5.2
4.3
3.4
2.5
N (cm⁻³)
15
10
5
0
N_cm3 H+
V (km/s)
5
0
−5
Vx H+
Vy H+
Vz H+
09:00
10:00
11:00
12:00
13:00
14:00
XGSE 2.26 2.64 2.78 2.53 1.82 0.79 −0.36
YGSE 0.65 −0.77 −2.12 −3.16 −3.62 −3.43 −2.79
ZGSE −5.81 −4.62 −3.03 −1.04 1.14 3.12 4.71
DIST 6.27 5.38 4.62 4.18 4.21 4.71 5.49

Figure 9

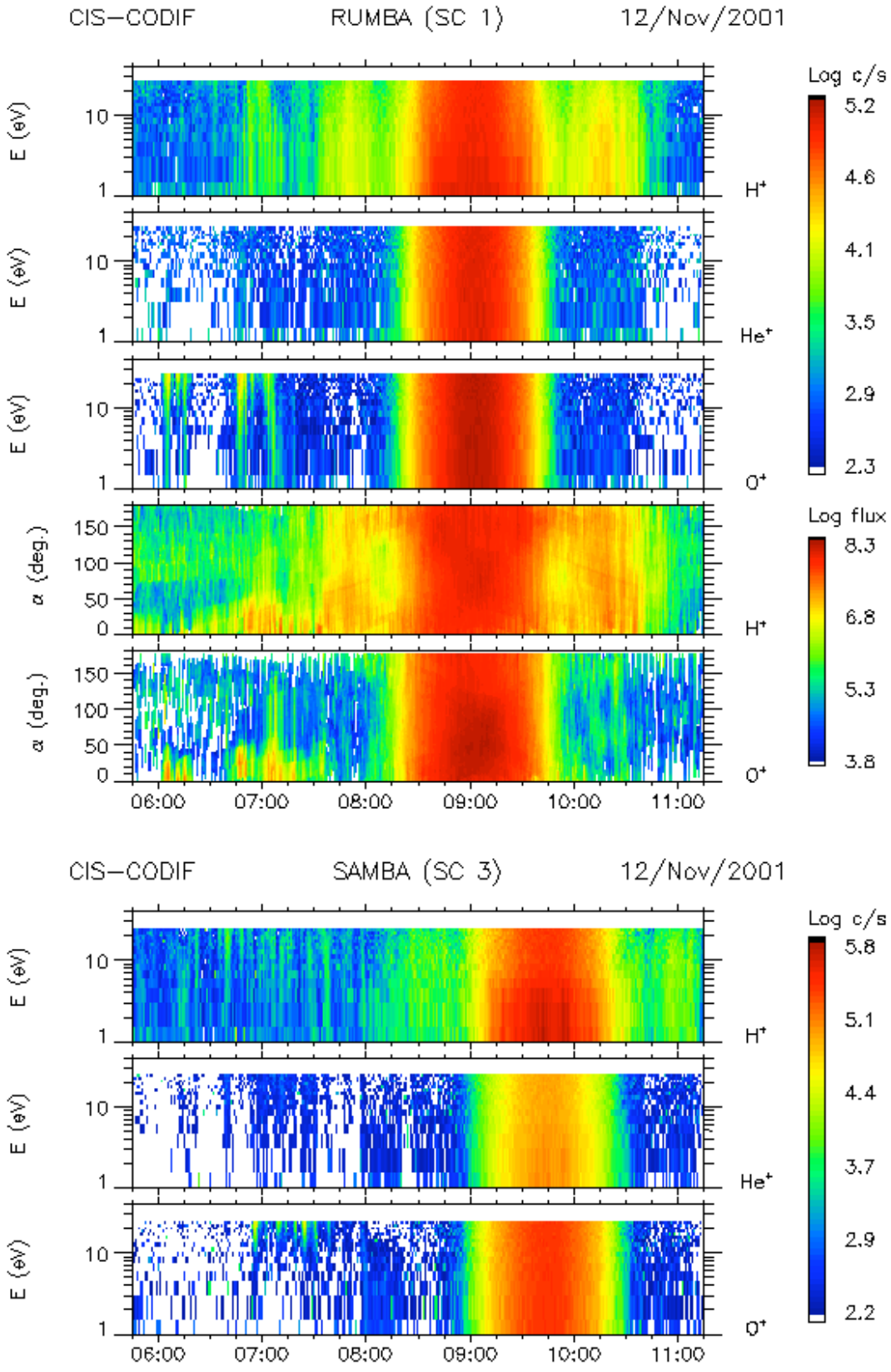
CIS–CODIF
RUMBA (SC 1)
12/Nov/2001
E (eV)
10
1
H+
He+
O+
α (deg.)
150
100
50
0
Log c/s
5.2
4.6
4.1
3.5
2.9
2.3
Log flux
8.3
6.8
5.3
3.8
06:00
07:00
08:00
09:00
10:00
11:00
CIS–CODIF
SAMBA (SC 3)
12/Nov/2001
5.8
5.1
4.4
3.7
2.9
2.2

Figure 10

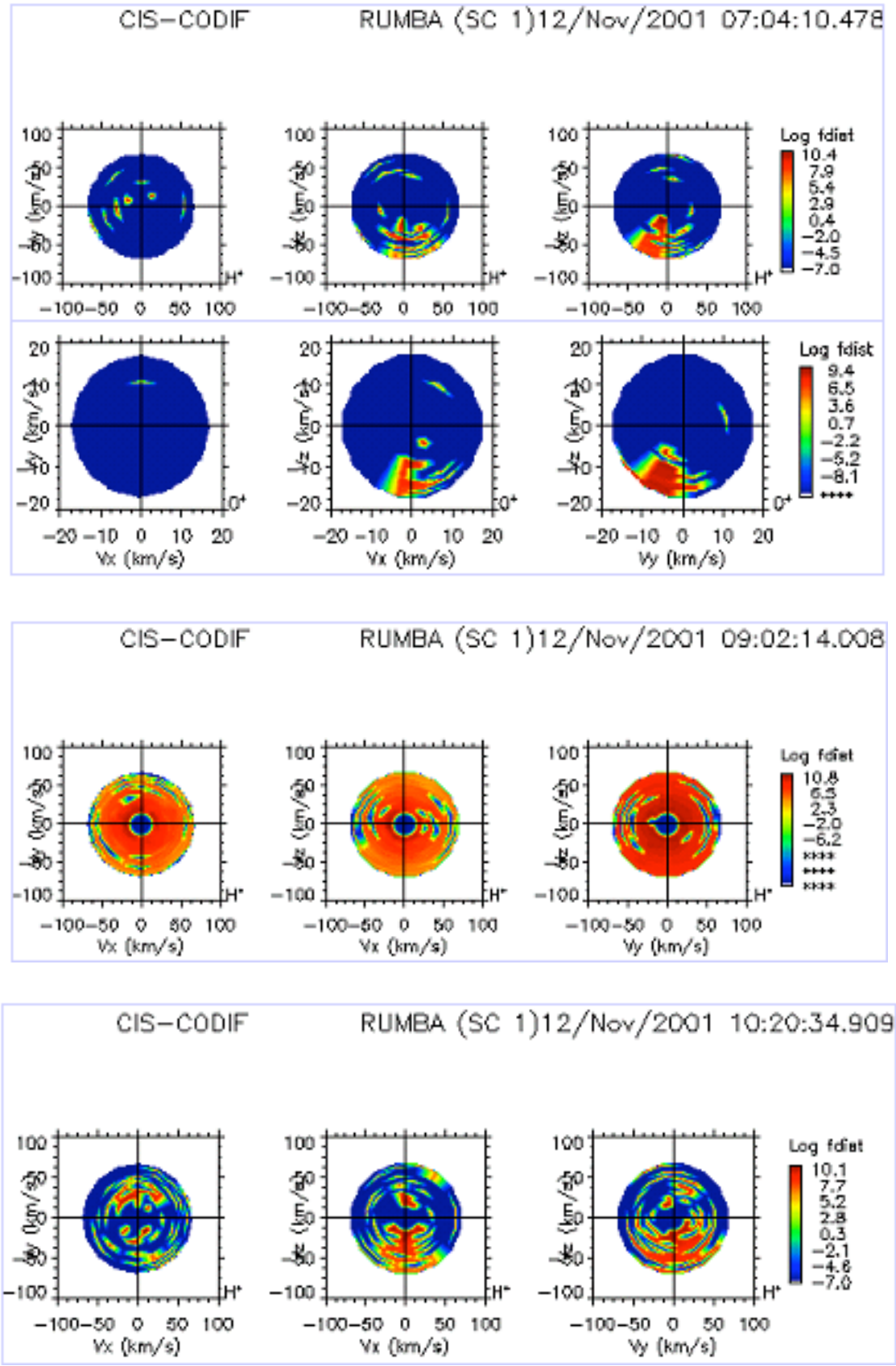
CIS-CODIF
RUMBA (SC 1)12/Nov/2001 07:04:10.478
Log fdist
10.4
7.9
5.4
2.9
0.4
-2.0
-4.5
-7.0
Log fdist
9.4
6.5
3.6
0.7
-2.2
-5.2
-8.1
Vx (km/s)
Vy (km/s)
CIS-CODIF
RUMBA (SC 1)12/Nov/2001 09:02:14.008
Log fdist
10.8
6.5
2.3
-2.0
-6.2
Vx (km/s)
Vy (km/s)
CIS-CODIF
RUMBA (SC 1)12/Nov/2001 10:20:34.909
Log fdist
10.1
7.7
5.2
2.8
0.3
-2.1
-4.6
-7.0
Vx (km/s)
Vy (km/s)

Figure 11

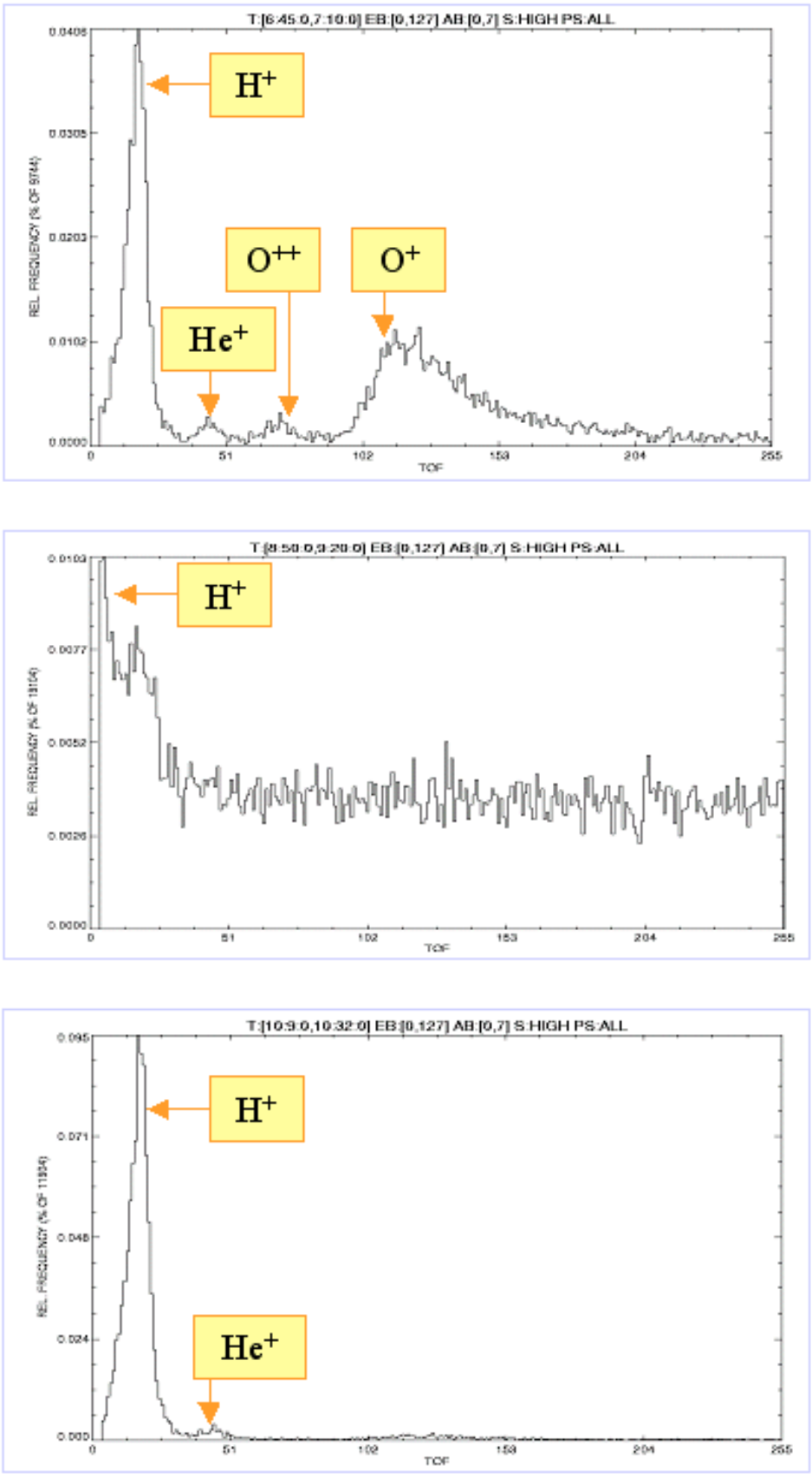
T:[6:45:0,7:10:0] EB:[0,127] AB:[0,7] S:HIGH PS:ALL
H+
O++
O+
He+
REL. FREQUENCY (% OF 9744)
TOF
T:[8:50:0,9:20:0] EB:[0,127] AB:[0,7] S:HIGH PS:ALL
H+
REL. FREQUENCY (% OF 19104)
TOF
T:[10:9:0,10:32:0] EB:[0,127] AB:[0,7] S:HIGH PS:ALL
H+
He+
REL. FREQUENCY (% OF 11934)
TOF

Figure 12

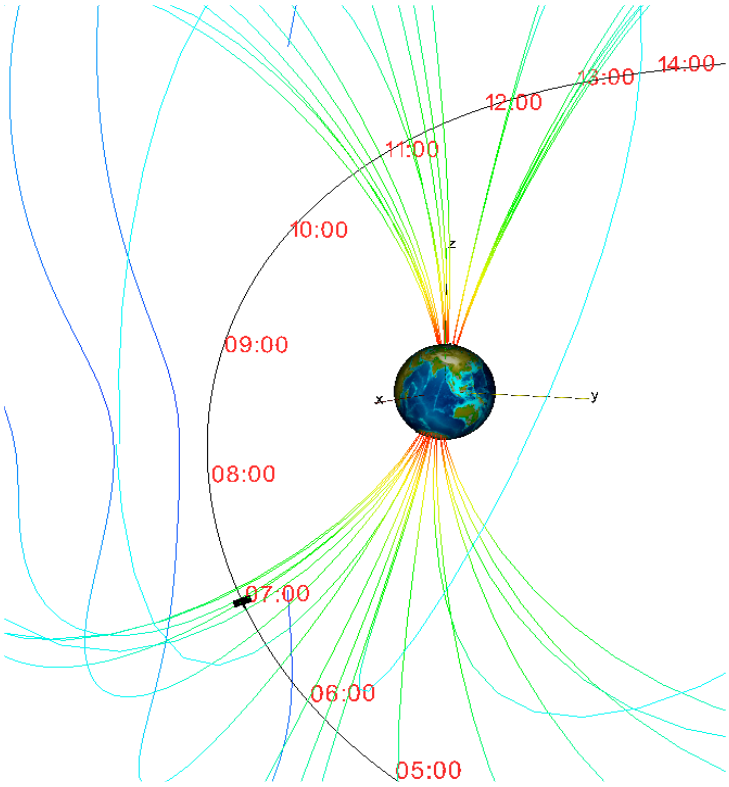

Figure 13

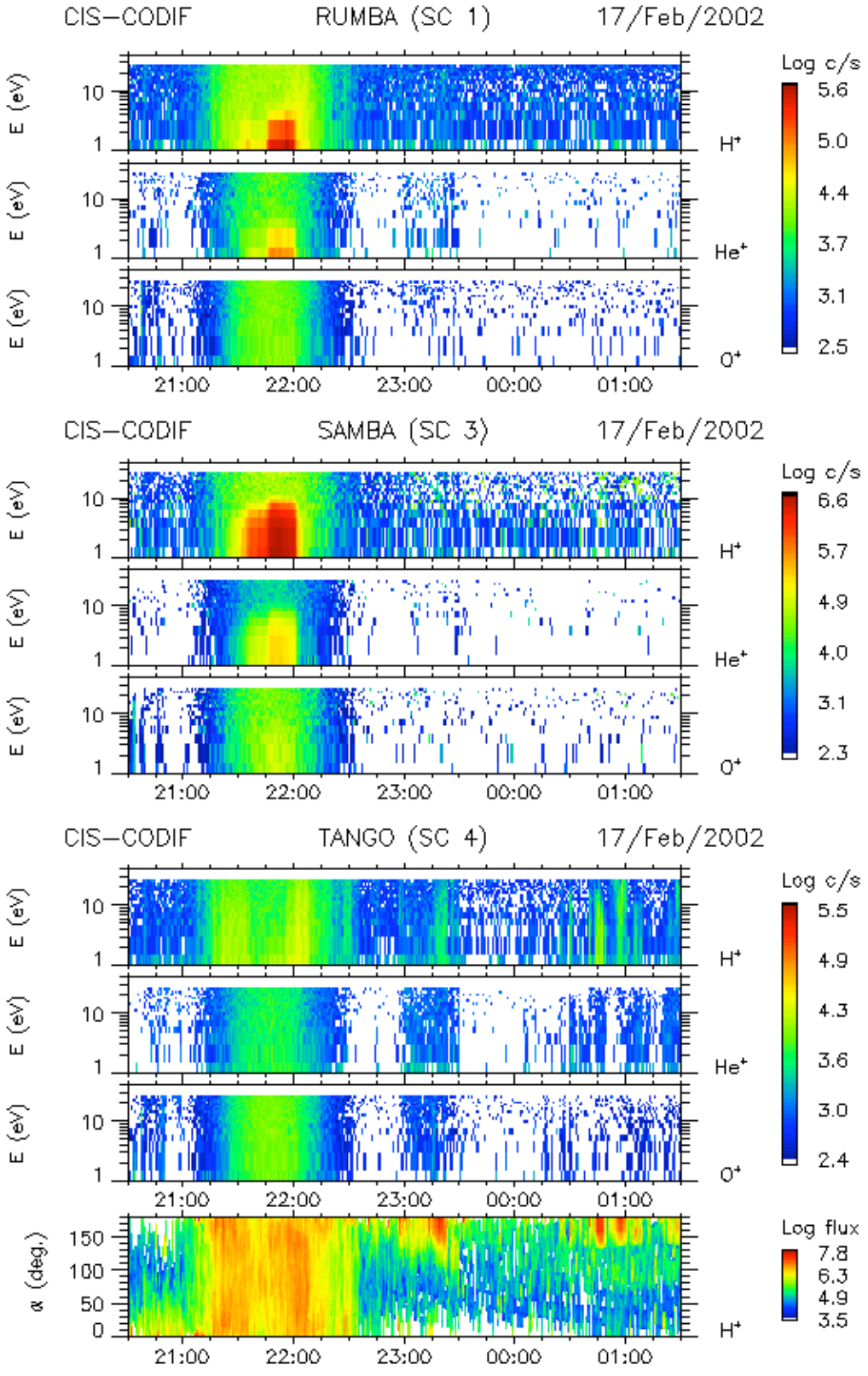
CIS–CODIF
RUMBA (SC 1)
17/Feb/2002
E (eV)
10
1
H+
He+
O+
21:00
22:00
23:00
00:00
01:00
Log c/s
5.6
5.0
4.4
3.7
3.1
2.5
CIS–CODIF
SAMBA (SC 3)
17/Feb/2002
6.6
5.7
4.9
4.0
3.1
2.3
CIS–CODIF
TANGO (SC 4)
17/Feb/2002
5.5
4.9
4.3
3.6
3.0
2.4
α (deg.)
150
100
50
0
Log flux
7.8
6.3
4.9
3.5

Figure 14

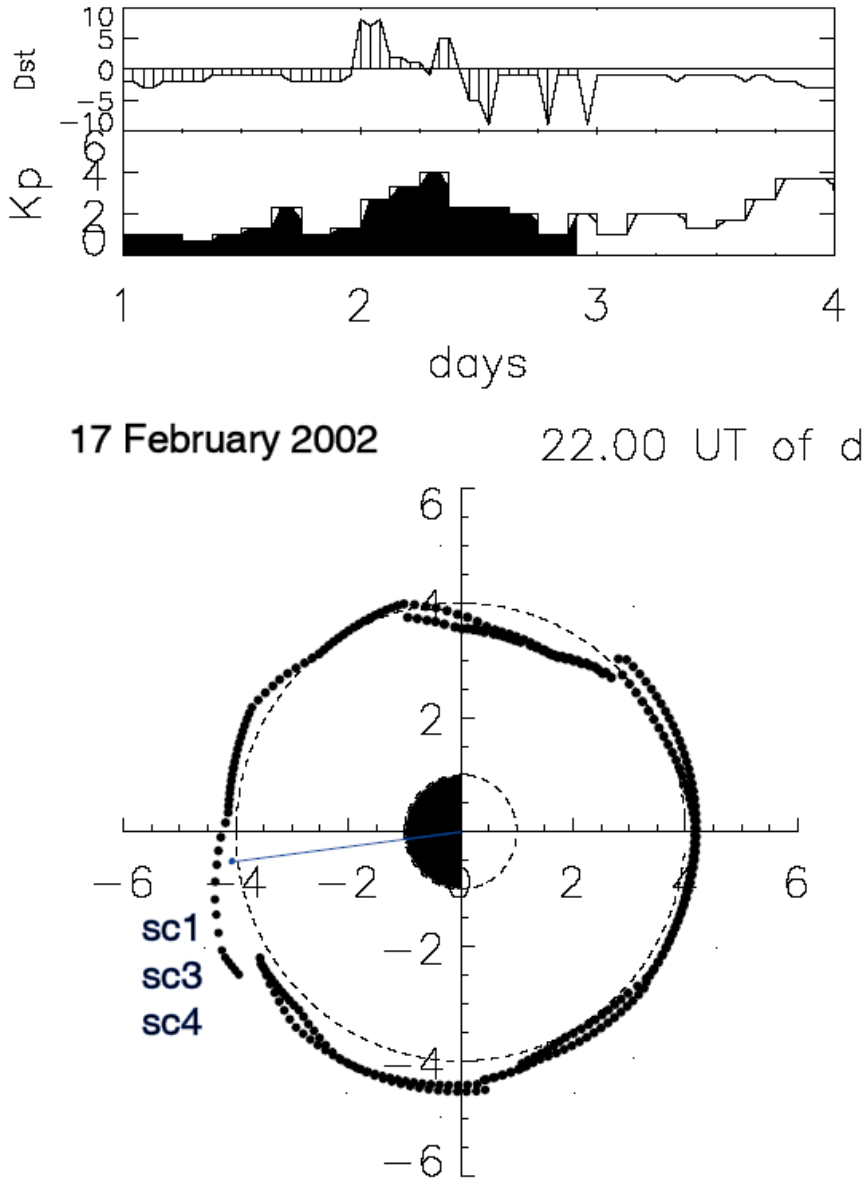
Dst
10
5
0
−5
−10
Kp
6
4
2
0
1
2
3
4
days
17 February 2002
22.00 UT of day 2
6
4
2
−2
−4
−6
−6
−4
−2
0
2
4
6
sc1
sc3
sc4

Figure 15

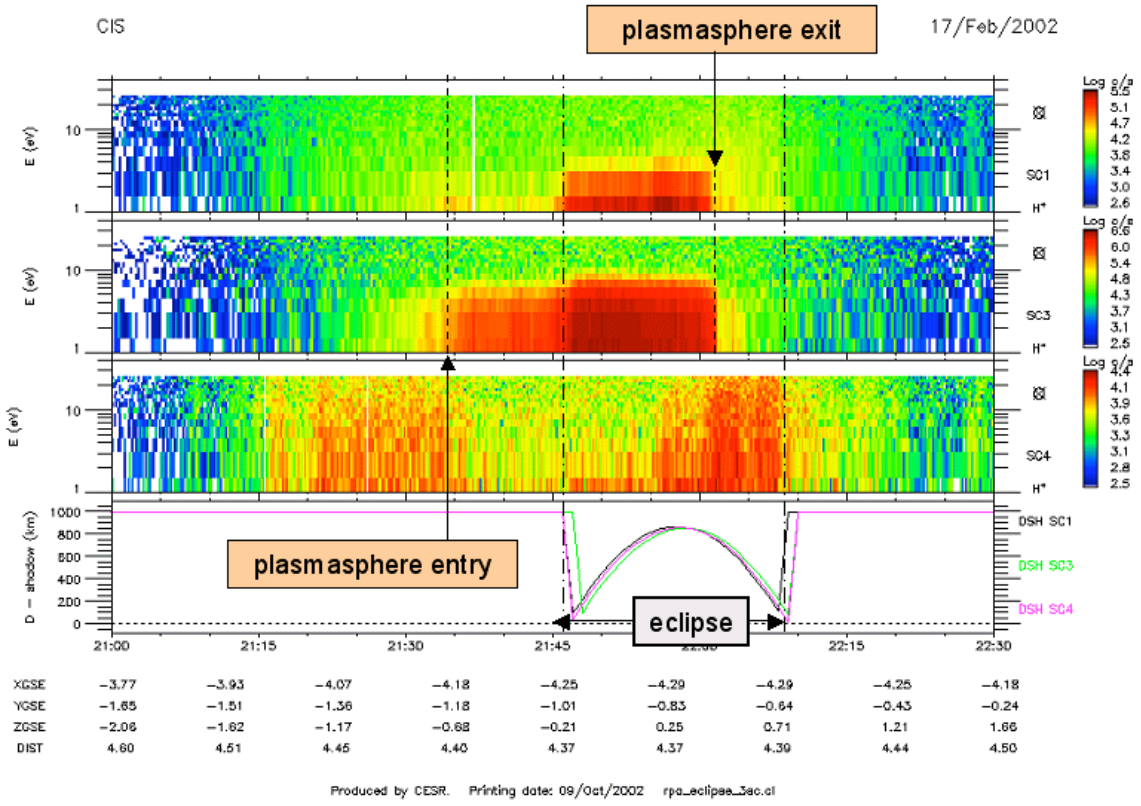
CIS
plasmasphere exit
17/Feb/2002
E (eV)
SC1
SC3
SC4
H+
D = shadow (km)
DSH SC1
DSH SC3
DSH SC4
plasmasphere entry
eclipse
21:00
21:15
21:30
21:45
22:15
22:30
XGSE −3.77 −3.93 −4.07 −4.18 −4.25 −4.29 −4.29 −4.25 −4.18
YGSE −1.65 −1.51 −1.36 −1.18 −1.01 −0.83 −0.64 −0.43 −0.24
ZGSE −2.06 −1.62 −1.17 −0.68 −0.21 0.25 0.71 1.21 1.66
DIST 4.60 4.51 4.45 4.40 4.37 4.37 4.39 4.44 4.50
Produced by CESR. Printing date: 09/Oct/2002 rpa_eclipse_3sc.ol

Figure 16

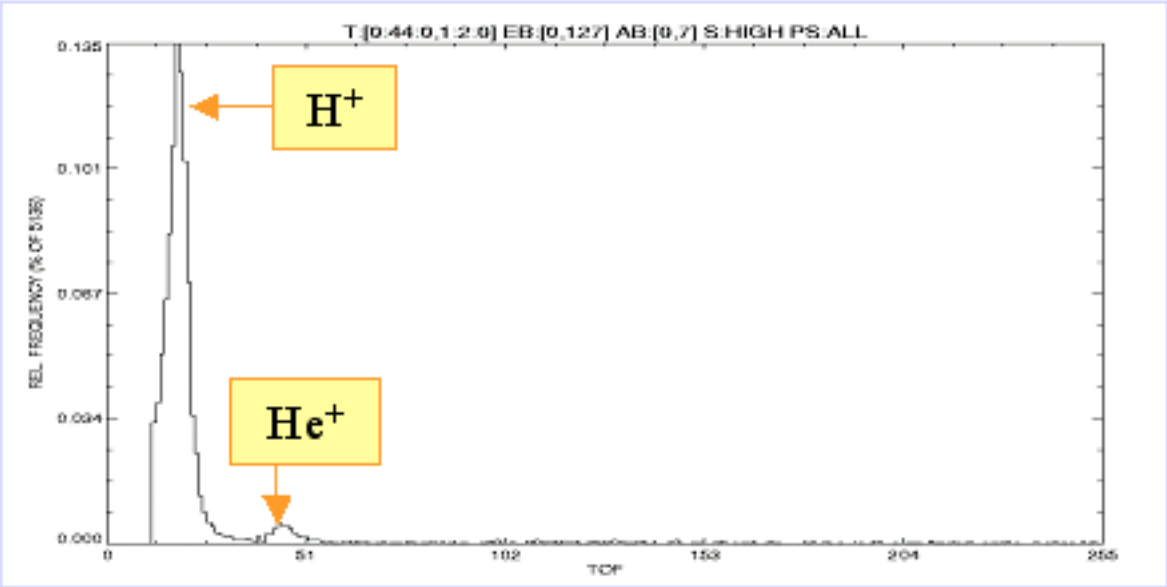
T:[0:44:0,1:2:0] EB:[0,127] AB:[0,7] S:HIGH PS:ALL
H+
He+
REL FREQUENCY (% OF 5136)
0.135
0.101
0.067
0.034
0.000
0
51
102
153
204
255
TOF

Figure 17

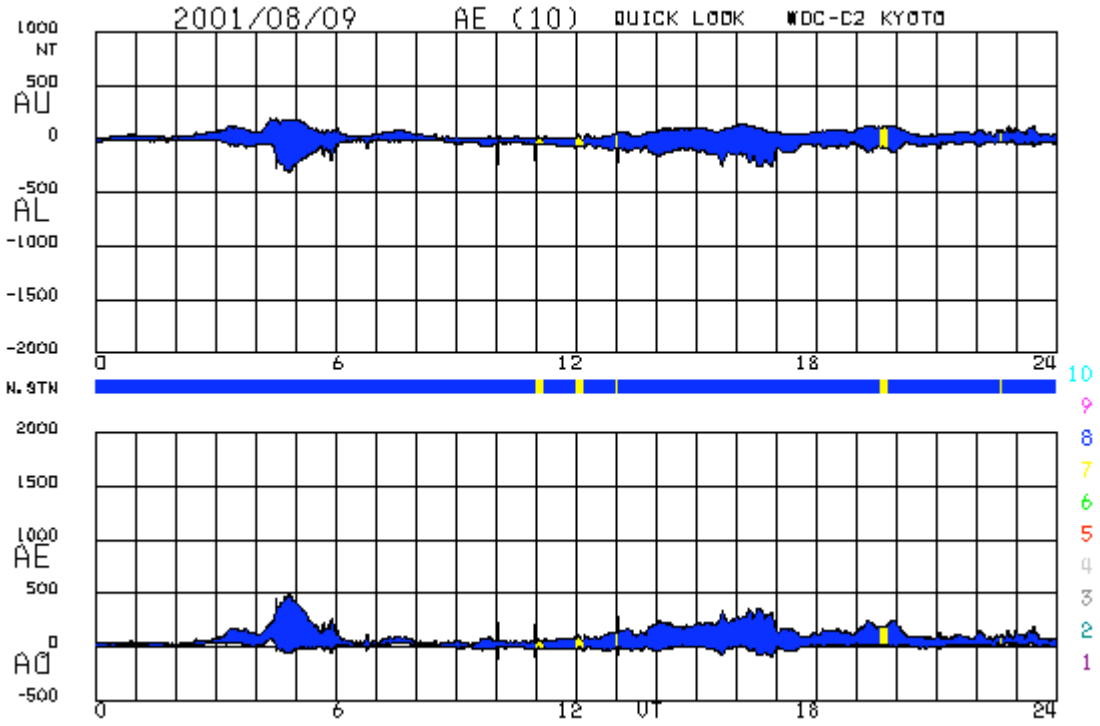
2001/08/09
AE (10)
QUICK LOOK
WDC-C2 KYOTO
1000
NT
500
AU
0
-500
AL
-1000
-1500
-2000
0
6
12
18
24
N.STN
10
9
8
7
6
5
4
3
2
1
2000
1500
1000
AE
500
0
AO
-500
0
6
12
UT
18
24

Figure 18

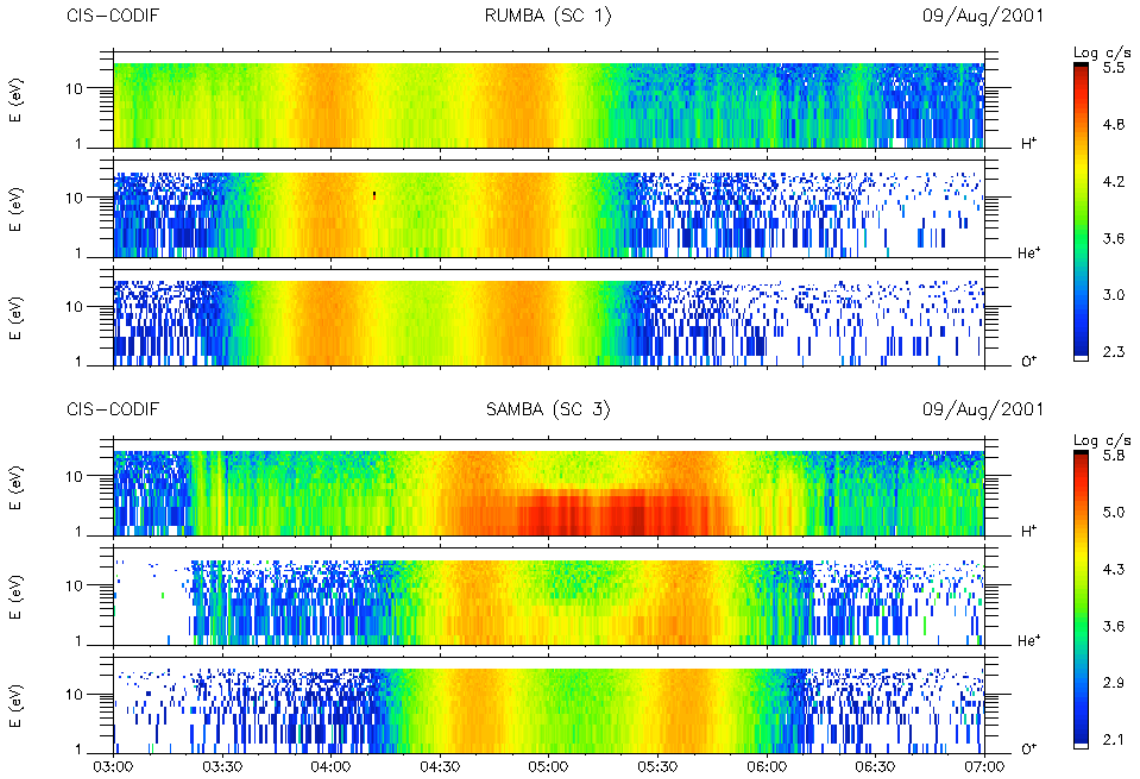
CIS–CODIF
RUMBA (SC 1)
09/Aug/2001
Log c/s
5.5
4.8
4.2
3.6
3.0
2.3
E (eV)
10
1
H+
He+
O+
CIS–CODIF
SAMBA (SC 3)
09/Aug/2001
Log c/s
5.8
5.0
4.3
3.6
2.9
2.1
03:00
03:30
04:00
04:30
05:00
05:30
06:00
06:30
07:00

Figure 19

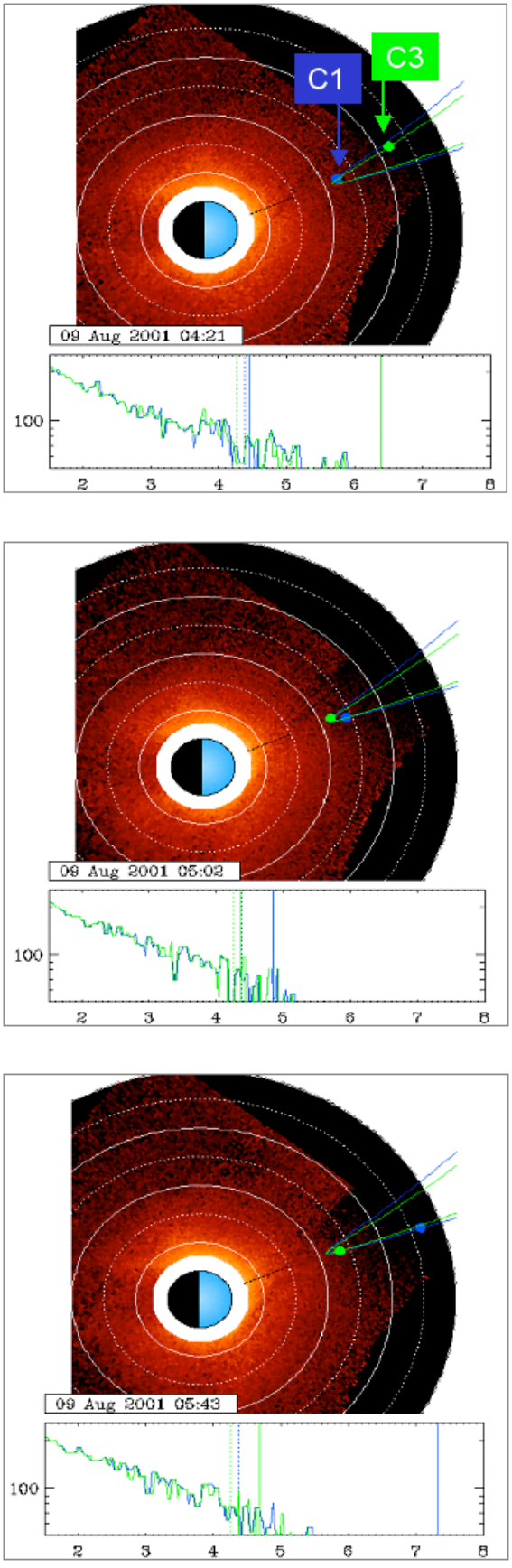
C1
C3
09 Aug 2001 04:21
100
2
3
4
5
6
7
8
09 Aug 2001 05:02
100
2
3
4
5
6
7
8
09 Aug 2001 05:43
100
2
3
4
5
6
7
8

Figure 20

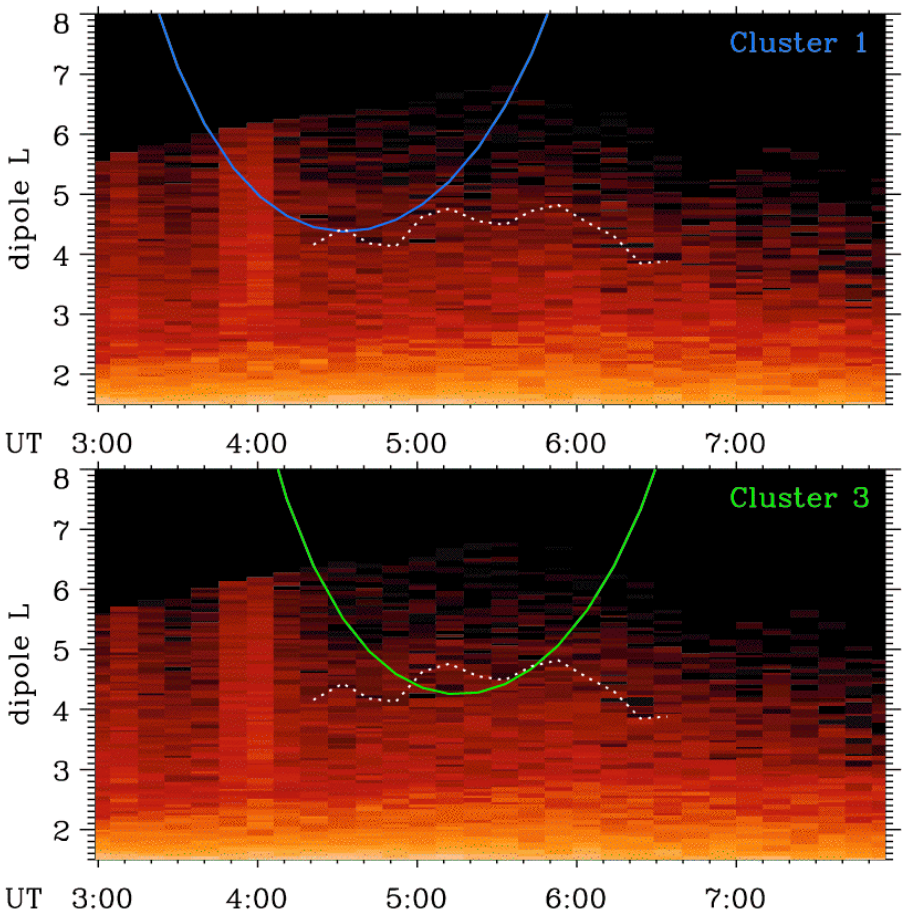
Cluster 1
dipole L
8
7
6
5
4
3
2
UT
3:00
4:00
5:00
6:00
7:00
Cluster 3
dipole L
8
7
6
5
4
3
2
UT
3:00
4:00
5:00
6:00
7:00

Figure 21

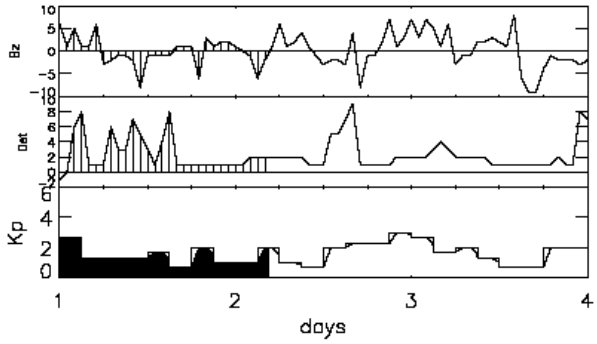
Bz
Dst
Kp
days

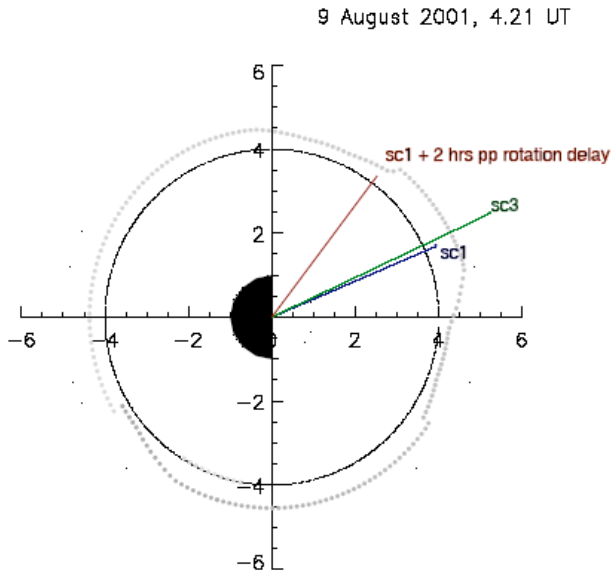
9 August 2001, 4.21 UT
sc1 + 2 hrs pp rotation delay
sc3
sc1

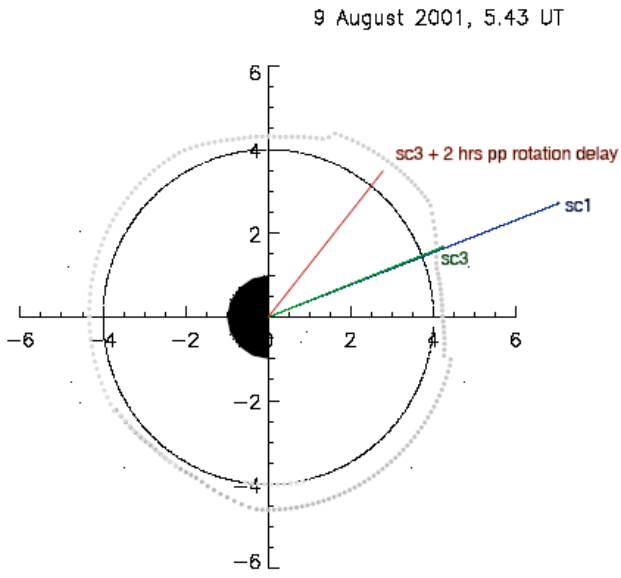
9 August 2001, 5.43 UT
sc3 + 2 hrs pp rotation delay
sc1
sc3

Figure 22

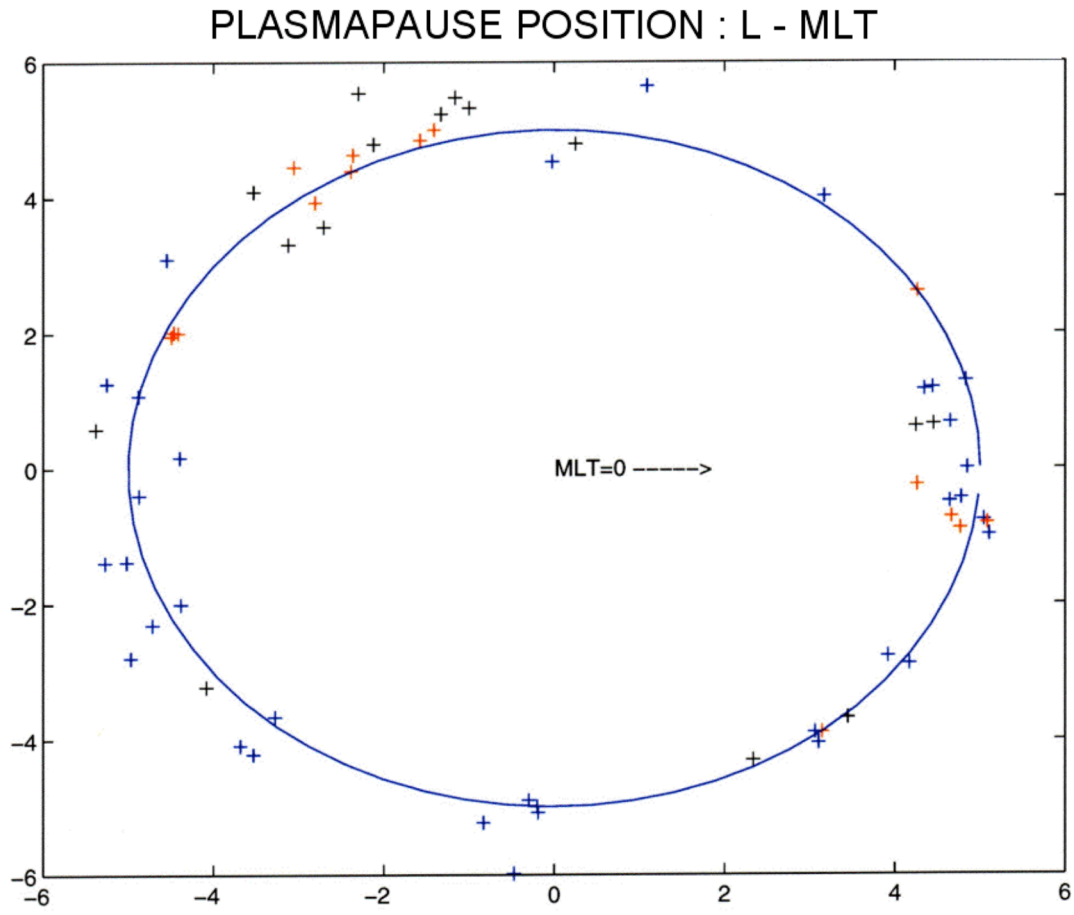

Figure 23

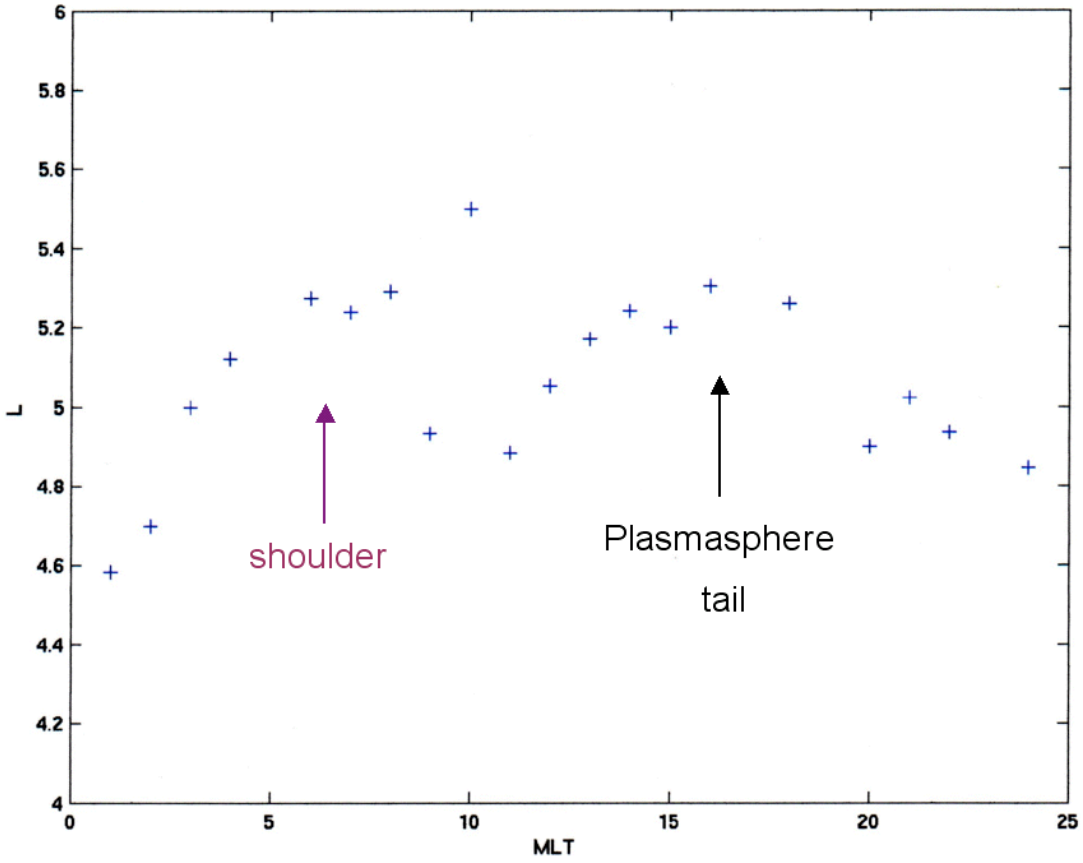
6
5.8
5.6
5.4
5.2
5
4.8
4.6
4.4
4.2
4
L
0
5
10
15
20
25
MLT
shoulder
Plasmasphere
tail

Figure 24

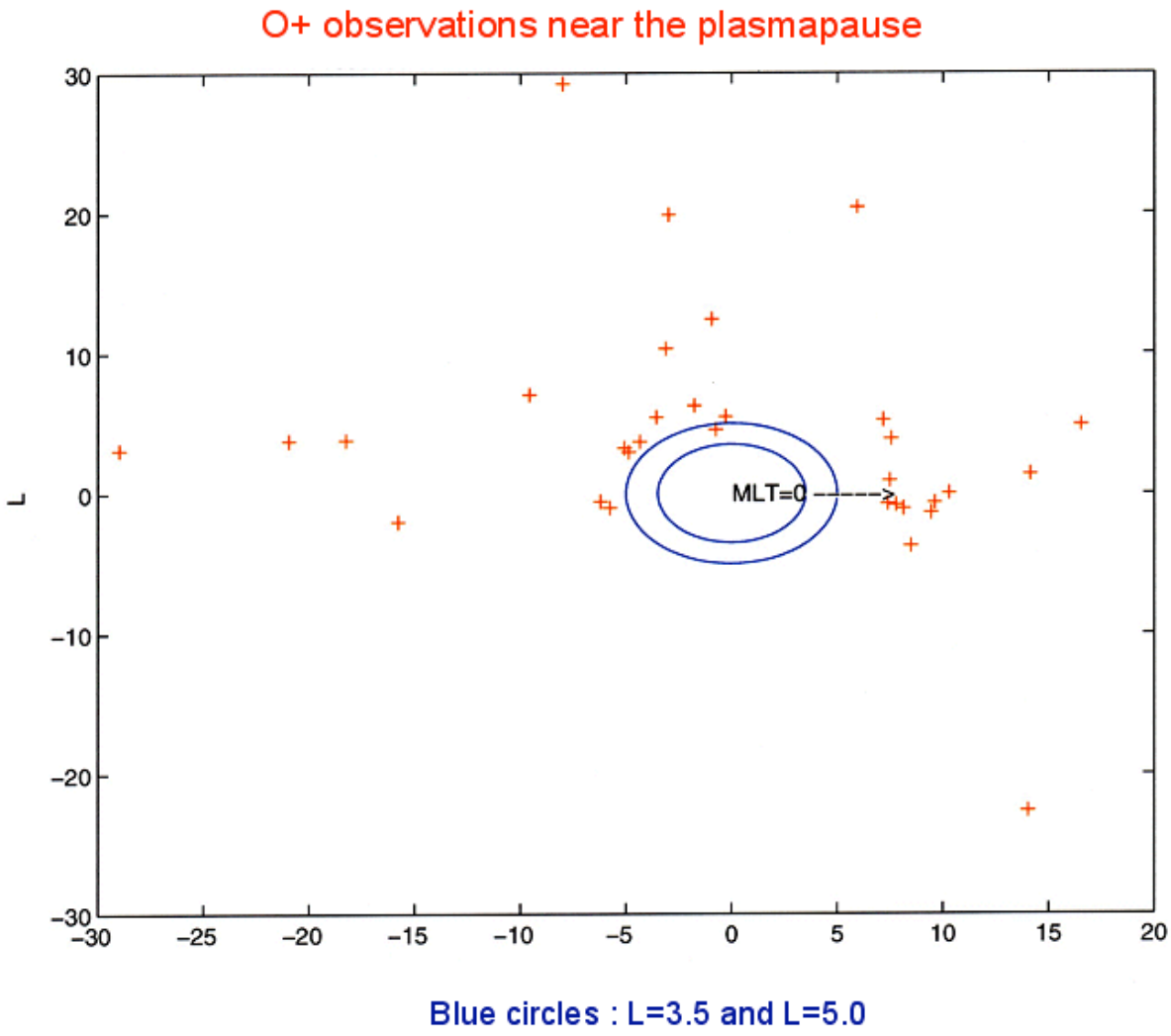
O+ observations near the plasmapause
L
MLT=0 ----->
Blue circles : L=3.5 and L=5.0

Figure 25